Geophys. J. Int. (2000) **141,** 157–174

Fréchet kernels for finite-frequency traveltimes—I. Theory

F. A. Dahlen, S.-H. Hung and Guust Nolet
Department of Geosciences, Princeton University, Princeton, NJ 08544, *USA. E-mail: fad@princeton.edu*

Accepted 1999 November 9. Received 1999 November 5; in original form 1999 May 14

SUMMARY

We use body wave ray theory in conjunction with the Born approximation to compute 3-D Fréchet kernels for finite-frequency seismic traveltimes, measured by cross-correlation of a broad-band waveform with a spherical earth synthetic seismogram. Destructive interference among adjacent frequencies in the broad-band pulse renders a cross-correlation traveltime measurement sensitive only to the wave speed in a hollow banana-shaped region surrounding the unperturbed geometrical ray. The Fréchet kernel expressing this sensitivity is expressed as a double sum over all forward-propagating body waves from the source and backward-propagating body waves from the receiver to every single scatterer in the vicinity of this central ray. The kernel for a differential traveltime, measured by cross-correlation of two phases at the same receiver, is simply the difference of the respective single-phase kernels. In the paraxial approximation, an absolute or differential traveltime kernel can be computed extremely economically by implementing a single kinematic and dynamic ray trace along each source-to-receiver ray.

Key words: body waves, Fréchet derivatives, global seismology, ray theory, tomography, traveltime.

1 INTRODUCTION

At the present time, geometrical ray theory is the basis of essentially all global seismic traveltime tomography (Dziewonski 1984; Inoue *et al.* 1990; Pulliam *et al.* 1993; Grand 1994; Van der Hilst *et al.* 1997). In that approximation, the arrival time of a body wave phase depends only upon the wave speed along the geometrical ray path between the source and receiver. In fact, ray theory is strictly valid only in the limit of a hypothetical infinite-frequency wave; scattering, wave-front healing and other diffraction effects render the traveltime of a finite-frequency seismic wave sensitive to 3-D structure off the ray. In all of the above-cited studies, an analyst or investigator has measured each traveltime by hand-picking the first break; the use of ray theory is generally justified by the argument that such a picked time corresponds to the arrival of the highest-frequency observable waves.

The widespread availability of broad-band digital data has led to the recent development of automated traveltime measurement techniques, based upon the cross-correlation of an observed body wave phase with the corresponding spherical earth synthetic phase (e.g. Su & Dziewonski 1992; Masters *et al.* 1996). Cross-correlation methods have also been used to measure the relative arrival times of a phase at a number of stations in a seismic array (VanDecar & Crosson 1990) and the differential traveltime of two phases at the same station (e.g. Kuo *et al.* 1987; Sheehan & Solomon 1991; Woodward & Masters 1991). In a previous publication, we explored the 3-D sensitivity of such absolute or differential cross-correlation traveltime measurements using a coupled surface wave version of the Born approximation (Marquering *et al.* 1999). Paradoxically, we found that the sensitivity of a finite-frequency teleseismic *S* wave is identically zero everywhere along the geometrical ray! The geometry of the 3-D Fréchet kernel resembles that of a hollow banana; in a cross-section perpendicular to the ray, the shape resembles a doughnut. The cross-path width of every such *banana–doughnut kernel* was found empirically to depend upon the frequency content of the wave.

In the present paper (Banana–Doughnut I) and its sequel (Hung *et al.* 2000, hereafter referred to as Banana–Doughnut II), we describe an alternative procedure for computing the Fréchet sensitivity kernel of a finite-frequency, cross-correlation traveltime. Instead of representing the kernel as a double sum over all possible source-to-scatterer and scatterer-to-receiver *surface waves*, as we did in Marquering *et al.* (1999), we represent it as a double sum over all scattered *body waves*. The resulting formulation is more general, inasmuch as it is applicable to waves of arbitrarily low ray parameter, including essentially vertically propagating multiple *PcP* and *ScS* waves. In addition, it is much more economical; an absolute traveltime kernel can be computed in the paraxial approximation by means of a single kinematic and dynamic ray trace along the unperturbed central ray. Perhaps most importantly, the new Born body wave formulation provides

a simple physical interpretation of many of the features of the absolute and differential kernels that were heretofore only empirical. In particular, the dependence upon the power spectrum of the cross-correlated pulse is now explicit; furthermore, the banana–doughnut character of a direct *P*-wave or *S*-wave kernel, as well as the more intricate geometry of a minimax *PP* or *SS* kernel, are simply explained.

2 PRELIMINARIES

Consider an isotropic elastic earth model occupying a volume $\oplus$ with surface $\partial\oplus$. Denote the density by ρ and the Lamé parameters by λ and μ; the compressional and shear wave speeds are given in terms of these properties by $\alpha=[(\lambda+2\mu)/\rho]^{1/2}$ and $\beta=(\mu/\rho)^{1/2}$, respectively. The model may have a number of internal solid–solid discontinuities, denoted by Σ_{SS}, and a number of internal fluid–solid discontinuities, denoted by Σ_{FS}. The union of all the boundaries, including the outer free surface $\partial\oplus$, will be denoted by $\Sigma=\partial\oplus\cup\Sigma_{SS}\cup\Sigma_{FS}$. The unit outward normal to Σ will be denoted by $\hat{\mathbf{n}}$; we use a $+$ and $-$ to refer to the outside and inside of Σ, respectively. In most global seismological applications, the unperturbed earth model $\oplus$ will be spherically symmetrical; that is, ρ, λ, μ and α, β will be piecewise continuous functions only of radius r, and the normal $\hat{\mathbf{n}}$ to Σ will be the unit radial vector $\hat{\mathbf{r}}$. In the general theory that follows, however, there is no need to assume this.

We shall, in the ensuing discussion, consider functions of both time t and angular frequency ω. Our Fourier sign convention is that adopted by Dahlen & Tromp (1998):

$$f(\omega)=\int_0^\infty f(t)\exp(-i\omega t)\,dt\,, \tag{1}$$

$$f(t)=\frac{1}{\pi}\,\mathscr{R}e\int_0^\infty f(\omega)\exp(i\omega t)\,d\omega\,, \tag{2}$$

for every function $f(t)$ of time that vanishes prior to $t=0$. We have used the symmetry relation $f(-\omega)=f^*(\omega)$, where the asterisk denotes the complex conjugate, to limit the integration in the inverse transform (2) to positive frequencies, $0\le\omega\le\infty$.

2.1 Equations of motion

Let $\mathbf{G}_{rs}(t)$ be the time-domain Green tensor, or displacement response of the earth model at the location $\mathbf{r}$ of a receiver to an impulsive force applied at time $t=0$ at a source point $\mathbf{s}$. To find this impulse response, we must solve a boundary-value problem of the form

$$\mathscr{L}\mathbf{G}_{rs}=\mathbf{0}\quad\text{in }\oplus\,, \tag{3}$$

$$[\mathscr{B}\mathbf{G}_{rs}]_-^+=\mathbf{0}\quad\text{on }\Sigma\,, \tag{4}$$

subject to the initial conditions

$$\mathbf{G}_{rs}(0)=\mathbf{0}\,,\qquad \partial_t\mathbf{G}_{rs}(0)=\rho^{-1}\mathbf{I}\,\delta(\mathbf{r}-\mathbf{s})\,, \tag{5}$$

where $\mathbf{I}$ is the identity tensor. The volumetric and boundary operators in (3)–(4) are defined by

$$\mathscr{L}\mathbf{G}_{rs}=\rho\,\partial_t^2\mathbf{G}_{rs}-\boldsymbol{\nabla}(\lambda\boldsymbol{\nabla}\cdot\mathbf{G}_{rs})-\boldsymbol{\nabla}\cdot\{\mu[\boldsymbol{\nabla}\mathbf{G}_{rs}+(\boldsymbol{\nabla}\mathbf{G}_{rs})^{\mathrm{T}}]\}\,, \tag{6}$$

$$\mathscr{B}\mathbf{G}_{rs}=\hat{\mathbf{n}}(\lambda\boldsymbol{\nabla}\cdot\mathbf{G}_{rs})+\hat{\mathbf{n}}\cdot\{\mu[\boldsymbol{\nabla}\mathbf{G}_{rs}+(\boldsymbol{\nabla}\mathbf{G}_{rs})^{\mathrm{T}}]\}\,. \tag{7}$$

The transposes in the representations (6)–(7) are over the first two indices, so that the components of $\mathscr{L}\mathbf{G}$, for example, are $\rho\,\partial_t^2G_{jk}-\partial_j(\lambda\partial_iG_{ik})-\partial_i[\mu(\partial_iG_{jk}+\partial_jG_{ik})]$. The Green tensor also satisfies the obvious kinematic continuity conditions $[\mathbf{G}_{rs}]_-^+=\mathbf{0}$ on Σ_{SS} and $[\hat{\mathbf{n}}\cdot\mathbf{G}_{rs}]_-^+=\mathbf{0}$ on Σ_{FS}.

2.2 Body wave Green tensor

As noted earlier, our analysis is grounded upon an approximate JWKB solution to eqs (3)–(7). In this approximation, the impulse response is expressed as a sum over all of the body waves that propagate from the source $\mathbf{s}$ to the receiver $\mathbf{r}$. We write the Fourier transform of the response $\mathbf{G}_{rs}(\omega)$ using a slightly modified version of the ray-theoretical notation employed by Dahlen & Tromp (1998, Sections 12.5 & 15.7):

$$\mathbf{G}_{rs}(\omega)=\frac{1}{4\pi}\sum_{\text{rays}}\hat{\mathbf{p}}_r\hat{\mathbf{p}}_s(\rho_r\rho_sc_rc_s^3)^{-1/2}\,\Pi_{rs}\,\mathscr{R}_{rs}^{-1}$$
$$\times\exp i(-\omega T_{rs}+M_{rs}\pi/2)\,. \tag{8}$$

The subscripts s and r, as in ρ_s and ρ_r, denote evaluation at the source $\mathbf{s}$ and the receiver $\mathbf{r}$. The generic symbol c is shorthand for the wave speed, either α or β; note that c_s and c_r need not be of the same character if there is a conversion anywhere along the geometrical ray path, as in the case of *sP* or *ScP*. The quantity Π_{rs} is the product of signed $\pm$(energy)$^{1/2}$ reflection and transmission coefficients at the various boundaries Σ encountered along the ray path, and $\mathscr{R}_{rs}$ is the geometrical spreading coefficient, analogous to the straight-ray source–receiver distance $\|\mathbf{r}-\mathbf{s}\|$ in a homogeneous medium. The phase delay, or argument of the exponential, depends upon the traveltime

$$T_{rs}=\int_{\mathbf{s}}^{\mathbf{r}}\frac{dl}{c} \tag{9}$$

between the source and receiver, and upon the Maslov index M_{rs}, which counts the number of $\pi/2$ phase shifts due to passage of the wave through caustics. The integral in eq. (9) is taken along all of the legs of a compound ray; the independent variable dl is the differential arclength. Finally, the unit vectors $\hat{\mathbf{p}}_s$ and $\hat{\mathbf{p}}_r$ are the polarization directions of the wave upon leaving the source and arriving at the receiver, respectively. The polarization of a *P* wave is in the direction of propagation, $\hat{\mathbf{p}}=\hat{\mathbf{k}}$, whereas that of an *S* wave is transverse to the propagation direction, i.e. $\hat{\mathbf{k}}\cdot\hat{\mathbf{p}}=0$, where $\hat{\mathbf{k}}$ is the unit wave vector. We denote the two independent shear wave polarizations by $\hat{\mathbf{q}}_1$ and $\hat{\mathbf{q}}_2$, and stipulate that the orthonormal triad of polarization vectors $\hat{\mathbf{q}}_1$, $\hat{\mathbf{q}}_2$, $\hat{\mathbf{k}}$ is right-handed: $(\hat{\mathbf{q}}_1\times\hat{\mathbf{q}}_2)\cdot\hat{\mathbf{k}}=1$. A sketch summarizing this polarization notation is given in Fig. 1. In

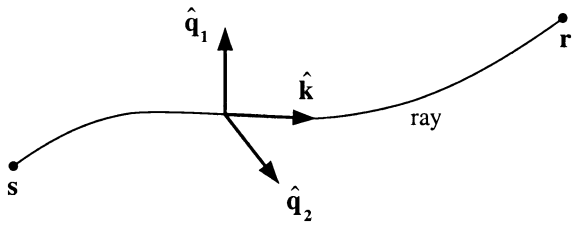

Figure 1. Cartoon of a geometrical ray from the source $\mathbf{s}$ to the receiver $\mathbf{r}$, showing the *P*-wave polarization, or unit wave vector, $\hat{\mathbf{k}}$, and the two transverse *S*-wave polarizations, $\hat{\mathbf{q}}_1$ and $\hat{\mathbf{q}}_2$.

a spherically symmetric earth model, the subscripts 1 and 2 are associated with *SV*-polarized and *SH*-polarized waves, respectively; that is, $\hat{\mathbf{q}}_1 = \hat{\mathbf{q}}_{SV}$ and $\hat{\mathbf{q}}_2 = \hat{\mathbf{q}}_{SH}$.

The traveltime and number of caustic passages are independent of whether the ray is traced from the source to the receiver or *vice versa*:

$$T_{\mathrm{rs}} = T_{\mathrm{sr}}\,, \qquad M_{\mathrm{rs}} = M_{\mathrm{sr}}\,. \tag{10}$$

The reflection–transmission coefficient product and geometrical spreading factor likewise satisfy the dynamical symmetries (Dahlen & Tromp 1998, Sections 12.1.6, 12.1.7, 15.4.6 and 15.6.3)

$$\Pi_{\mathrm{rs}} = \Pi_{\mathrm{sr}}\,, \qquad c_{\mathrm{s}}\mathscr{R}_{\mathrm{rs}} = c_{\mathrm{r}}\mathscr{R}_{\mathrm{sr}}\,. \tag{11}$$

Taken together, the results (10)–(11) guarantee that the JWKB body wave Green tensor (8) satisfies the principle of source–receiver reciprocity: $\mathbf{G}_{\mathrm{sr}} = \mathbf{G}_{\mathrm{rs}}^{\mathrm{T}}$.

The time-domain Green tensor obtained by inverse Fourier transformation of (8) is a sum of propagating pulses:

$$\mathbf{G}_{\mathrm{rs}}(t) = \frac{1}{4\pi}\sum_{\mathrm{rays}} \hat{\mathbf{p}}_{\mathrm{r}}\hat{\mathbf{p}}_{\mathrm{s}}(\rho_{\mathrm{r}}\rho_{\mathrm{s}}c_{\mathrm{r}}c_{\mathrm{s}}^3)^{-1/2}\,\Pi_{\mathrm{rs}}\,\mathscr{R}_{\mathrm{rs}}^{-1}\,\delta_{\mathrm{H}}^{(M_{\mathrm{rs}})}(t-T_{\mathrm{rs}})\,. \tag{12}$$

The symbol $\delta_{\mathrm{H}}^{(M)}(t)$ denotes the M-times Hilbert transform of the Dirac delta function, given by

$$\delta_{\mathrm{H}}^{(M)}(t) = \frac{1}{\pi}\,\mathscr{R}e\int_0^\infty \exp i(\omega t + M\pi/2)\,d\omega\,. \tag{13}$$

Each passage of a wave through a caustic acts to Hilbert transform the initial far-field pulse $\delta(t)$. The first two distorted pulses are $\delta_{\mathrm{H}}^{(1)}(t) = -(\pi t)^{-1}$ and $\delta_{\mathrm{H}}^{(2)}(t) = -\delta(t)$.

2.3 Moment tensor response

We model an earthquake as a temporally extended, synchronous point source situated at the point **s**, with a moment-rate tensor of the form

$$\dot{\mathbf{M}}(t) = \sqrt{2}M_0\hat{\mathbf{M}}\dot{m}(t)\,. \tag{14}$$

The quantity M_0 is the scalar moment, $\hat{\mathbf{M}}$ is the unit source mechanism tensor, satisfying $\hat{\mathbf{M}}:\hat{\mathbf{M}} = 1$, and $\dot{m}(t)$ is the normalized source time function, satisfying

$$\int_{t_0}^{t_{\mathrm{f}}} \dot{m}(t)\,dt = 1\,, \tag{15}$$

where t_0 and t_{f} are the start and end times of rupture, respectively. The frequency-domain response to such a source is given in terms of the body wave Green tensor $\mathbf{G}_{\mathrm{rs}}(\omega)$ by (Dahlen & Tromp 1998, Sections 12.5.5 and 15.7.2)

$$s(\omega) = \sqrt{2}M_0(i\omega)^{-1}\dot{m}(\omega)\hat{\mathbf{v}}\cdot[\hat{\mathbf{M}}:\boldsymbol{\nabla}_{\mathrm{s}}\mathbf{G}_{\mathrm{rs}}^{\mathrm{T}}(\omega)]\,. \tag{16}$$

The quantity $s(\omega)$ is the $\hat{\mathbf{v}}$ component of the ground displacement at the receiver **r** due to the earthquake at **s**, and $\dot{m}(\omega)$ is the Fourier transform of the source time function:

$$\dot{m}(\omega) = \int_{t_0}^{t_{\mathrm{f}}} \dot{m}(t)\exp(-i\omega t)\,dt\,. \tag{17}$$

In the JWKB approximation, the gradient $\boldsymbol{\nabla}_{\mathrm{s}}$ with respect to the source coordinates **s** in eq. (16) acts only upon the rapidly oscillating exponential $\exp(-i\omega T_{\mathrm{rs}})$ in (8), yielding a multiplier $\boldsymbol{\nabla}_{\mathrm{s}} \to i\omega c_{\mathrm{s}}^{-1}\hat{\mathbf{k}}_{\mathrm{s}}$. Upon collecting the source and receiver terms into factors

$$\Lambda = \sqrt{2}M_0(\rho_{\mathrm{s}}c_{\mathrm{s}}^5)^{-1/2}\,\hat{\mathbf{M}}:\frac{1}{2}\,(\hat{\mathbf{k}}_{\mathrm{s}}\hat{\mathbf{p}}_{\mathrm{s}} + \hat{\mathbf{p}}_{\mathrm{s}}\hat{\mathbf{k}}_{\mathrm{s}})\,, \tag{18}$$

$$\Upsilon = (\rho_{\mathrm{r}}c_{\mathrm{r}})^{-1/2}(\hat{\mathbf{v}}\cdot\hat{\mathbf{p}}_{\mathrm{r}})\,, \tag{19}$$

we can write the frequency-domain moment tensor response in the form (Dahlen & Tromp 1998, Sections 12.5.5 and 15.7.2)

$$s(\omega) = \frac{1}{4\pi}\sum_{\mathrm{rays}} \Lambda\Upsilon\Pi_{\mathrm{rs}}\mathscr{R}_{\mathrm{rs}}^{-1}\dot{m}(\omega)\exp i(-\omega T_{\mathrm{rs}} + M_{\mathrm{rs}}\pi/2)\,. \tag{20}$$

The corresponding displacement in the time domain obtained by inverse Fourier transformation of (20) is

$$s(t) = \frac{1}{4\pi}\sum_{\mathrm{rays}} \Lambda\Upsilon\Pi_{\mathrm{rs}}\mathscr{R}_{\mathrm{rs}}^{-1}\dot{m}_{\mathrm{H}}^{(M_{\mathrm{rs}})}(t-T_{\mathrm{rs}})\,. \tag{21}$$

The pulse shape of all least-time arrivals such as *P* and *S* is the source time function $\dot{m}(t)$; every passage through a caustic acts to Hilbert transform this far-field source time function. The quantity $\hat{\mathbf{M}}:\frac{1}{2}(\hat{\mathbf{k}}_{\mathrm{s}}\hat{\mathbf{p}}_{\mathrm{s}} + \hat{\mathbf{p}}_{\mathrm{s}}\hat{\mathbf{k}}_{\mathrm{s}})$ is the radiation pattern of the outgoing waves upon the focal sphere surrounding the source.

Anelastic attenuation and the associated dispersion can be accounted for by allowing the wave speed to be complex:

$$c \to c_0\left[1 + \frac{1}{2}\,iQ_c^{-1} + \frac{1}{\pi}\,Q_c^{-1}\ln(\omega/\omega_0)\right], \tag{22}$$

where c_0 is the speed—either α_0 or β_0—at the reference frequency ω_0, and Q_c denotes either the *P*-wave quality factor Q_α or the *S*-wave quality factor Q_β. We ignore the effect of attenuation upon the ray geometry, but incorporate its effect upon the complex traveltime by substituting for the Fourier transform of the source time function in the frequency-domain ray sum (20):

$$\dot{m}(\omega) \to \dot{m}(\omega)\exp i\omega\left[\frac{1}{2}\,iT_{\mathrm{rs}}^* + \frac{1}{\pi}\,T_{\mathrm{rs}}^*\ln(\omega/\omega_0)\right], \tag{23}$$

where

$$T_{\mathrm{rs}}^* = \int_{\mathbf{s}}^{\mathbf{r}} \frac{dl}{c_0 Q_c} \tag{24}$$

is the attenuation time. The resulting damping, broadening and delay of the time-domain pulse can be accounted for by convolution with a causal attenuation operator:

$$\dot{m}(t) \to \dot{m}(t) \tag{25}$$

$$* \frac{1}{\pi}\,\mathscr{R}e\int_0^\pi \exp i\omega\left[t + \frac{1}{2}\,iT_{\mathrm{rs}}^* + \frac{1}{\pi}\,T_{\mathrm{rs}}^*\ln(\omega/\omega_0)\right]d\omega\,.$$

We shall henceforth assume that $\dot{m}(\omega)$ and $\dot{m}(t)$ have been anelastically altered in accordance with (23) and (25). The altered spectrum and pulse shape are path-dependent; however, we shall not bother to revise the notation to reflect this.

3 BORN APPROXIMATION

Suppose now that the density and Lamé parameters of the earth model are subjected to an infinitesimal perturbation:

$$\rho \to \rho + \delta\rho\,, \qquad \lambda \to \lambda + \delta\lambda\,, \qquad \mu \to \mu + \delta\mu\,. \tag{26}$$

The associated perturbations in the compressional and shear wave speeds are given by

$$2\rho\alpha\,\delta\alpha = \delta\lambda + 2\,\delta\mu - \delta\rho\,\alpha^2\,, \qquad 2\rho\beta\,\delta\beta = \delta\mu - \delta\rho\,\beta^2\,. \tag{27}$$

We restrict attention in the present pair of papers to a strictly volumetric perturbation of the form (26)–(27). The locations of the boundaries Σ and the associated unit normals $\hat{\mathbf{n}}$ are assumed to be fixed. As already noted, the unperturbed parameters ρ, λ, μ and α, β in most global seismological applications will be spherical; the perturbations $\delta\rho$, $\delta\lambda$, $\delta\mu$ and $\delta\alpha$, $\delta\beta$ in that case represent the earth's unknown *3-D heterogeneity*.

3.1 Perturbed Green tensor

The volumetric and boundary operators (6)–(7) and the Green tensors (8) and (12) are altered as a result of the perturbations to the earth model:

$$\mathscr{L} \to \mathscr{L} + \delta\mathscr{L}\,, \qquad \mathscr{B} \to \mathscr{B} + \delta\mathscr{B}\,, \tag{28}$$

$$\mathbf{G}_{\rm rs} \to \mathbf{G}_{\rm rs} + \boldsymbol{\delta}\mathbf{G}_{\rm rs}\,. \tag{29}$$

We can find the perturbation to the Green tensor $\boldsymbol{\delta}\mathbf{G}_{\rm rs}$ correct to first order in $\delta\rho$, $\delta\lambda$ and $\delta\mu$ using the Born approximation. In the time domain, we are required to solve an inhomogeneous version of (3)–(4):

$$\mathscr{L}\,\boldsymbol{\delta}\mathbf{G}_{\rm rs} = -\delta\mathscr{L}\,\mathbf{G}_{\rm rs} \quad \text{in } \oplus\,, \tag{30}$$

$$[\mathscr{B}\,\boldsymbol{\delta}\mathbf{G}_{\rm rs}]^+_- = -[\delta\mathscr{B}\,\mathbf{G}_{\rm rs}]^+_- \quad \text{on } \Sigma\,, \tag{31}$$

subject to the initial conditions

$$\boldsymbol{\delta}\mathbf{G}_{\rm rs}(0) = \mathbf{0}\,, \qquad \partial_t \boldsymbol{\delta}\mathbf{G}_{\rm rs}(0) = \mathbf{0}\,. \tag{32}$$

The right sides of (30) and (31) may be regarded as specified body and surface forces acting within $\oplus$ and upon Σ, respectively; the solution is simply the superposition of the responses to these applied forces. To avoid an additional convolution over time, it is convenient to express the solution (via the substitution $\partial_t^2 \to -\omega^2$) in the frequency domain:

$$\boldsymbol{\delta}\mathbf{G}_{\rm rs} = -\iiint_{\oplus} [\mathbf{G}_{\rm rx} \cdot \delta\mathscr{L}\,\mathbf{G}_{\rm xs}]\,d^3\mathbf{x} + \iint_{\Sigma} [\mathbf{G}_{\rm rx} \cdot \delta\mathscr{B}\,\mathbf{G}_{\rm xs}]^+_-\,d^2\mathbf{x}\,, \tag{33}$$

where

$$\delta\mathscr{L}\,\mathbf{G}_{\rm xs} = -\omega^2\,\delta\rho\,\mathbf{G}_{\rm xs} - \boldsymbol{\nabla}(\delta\lambda\,\boldsymbol{\nabla}\cdot\mathbf{G}_{\rm xs}) - \boldsymbol{\nabla}\cdot\{\delta\mu[\boldsymbol{\nabla}\mathbf{G}_{\rm xs} + (\boldsymbol{\nabla}\mathbf{G}_{\rm xs})^{\rm T}]\}\,, \tag{34}$$

$$\delta\mathscr{B}\,\mathbf{G}_{\rm xs} = \hat{\mathbf{n}}(\delta\lambda\,\boldsymbol{\nabla}\cdot\mathbf{G}_{\rm xs}) + \hat{\mathbf{n}}\cdot\{\delta\mu[\boldsymbol{\nabla}\mathbf{G}_{\rm xs} + (\boldsymbol{\nabla}\mathbf{G}_{\rm xs})^{\rm T}]\}\,. \tag{35}$$

The spatial integration variable $\mathbf{x}$ in this representation of $\boldsymbol{\delta}\mathbf{G}_{\rm rs}(\omega)$ may be considered to range over all point scatterers within $\oplus$ and on Σ. All three perturbations $\delta\rho$, $\delta\lambda$, $\delta\mu$ in (34)–(35) are evaluated at the location of the scatterer $\mathbf{x}$, and all of the spatial gradients $\boldsymbol{\nabla}$ are $\boldsymbol{\nabla}_{\rm x}$. Gauss' theorem can be used to eliminate the derivatives of the model parameters $\delta\rho$, $\delta\lambda$ and $\delta\mu$ in the volume integral over $\oplus$. The surface integrals over Σ in eq. (33) are cancelled by the corresponding integrals that arise in this integration by parts, yielding

$$\boldsymbol{\delta}\mathbf{G}_{\rm rs} = \iiint_{\oplus} \delta\rho\,(\omega^2\mathbf{G}_{\rm rx}\cdot\mathbf{G}_{\rm xs})\,d^3\mathbf{x} - \iiint_{\oplus} \delta\lambda\,(\boldsymbol{\nabla}\cdot\mathbf{G}_{\rm rx}^{\rm T})(\boldsymbol{\nabla}\cdot\mathbf{G}_{\rm xs})\,d^3\mathbf{x} - \iiint_{\oplus} \delta\mu\,(\boldsymbol{\nabla}\mathbf{G}_{\rm rx})^{\rm T} : [\boldsymbol{\nabla}\mathbf{G}_{\rm xs} + (\boldsymbol{\nabla}\mathbf{G}_{\rm xs})^{\rm T}]\,d^3\mathbf{x}\,, \tag{36}$$

where the double contraction as well as all of the transposes are over the first two indices.

The result (36) does not depend upon the specific forms of the source-to-scatterer and scatterer-to-receiver Green tensors $\mathbf{G}_{\rm xs}(\omega)$ and $\mathbf{G}_{\rm rx}(\omega)$; in fact, we used precisely this result, together with a surface wave representation of these two unperturbed Green tensors, to obtain the cross-correlation traveltime kernels in Marquering *et al.* (1999). As noted in the Introduction, we switch to a body wave ray sum representation of $\mathbf{G}_{\rm xs}(\omega)$ and $\mathbf{G}_{\rm rx}(\omega)$ here. Upon substituting (8) and allowing the gradient $\boldsymbol{\nabla} = \boldsymbol{\nabla}_{\rm x}$ to operate only upon the rapidly oscillating exponentials $\exp(-i\omega T_{\rm xs})$ and $\exp(-i\omega T_{\rm rx})$, in accordance with the JWKB approximation, we can recast (36) into the convenient form (Hudson 1977; Wu & Aki 1985; Zhao & Dahlen 1996)

$$\boldsymbol{\delta}\mathbf{G}_{\rm rs}(\omega) = \omega^2 \iiint_{\oplus} [\mathbf{G}_{\rm rx}(\omega)\cdot(\rho\,\mathbf{S})\cdot\mathbf{G}_{\rm xs}(\omega)]\,d^3\mathbf{x}\,, \tag{37}$$

where the quantity $\mathbf{S} = \mathbf{S}_{\rm xx}$ is a second-order tensor that encapsulates all of the details regarding the scattering of an incoming body wave into an outgoing wave at the point $\mathbf{x}$. We can utilize the relations (27) to express this *scattering tensor* in terms of the wave speed and density perturbations $\delta\alpha$, $\delta\beta$ and $\delta\rho$ rather than $\delta\lambda$, $\delta\mu$ and $\delta\rho$:

$$\mathbf{S} = \left(\frac{\delta\alpha}{\alpha}\right)\mathbf{S}_\alpha + \left(\frac{\delta\beta}{\beta}\right)\mathbf{S}_\beta + \left(\frac{\delta\rho}{\rho}\right)\mathbf{S}_\rho\,, \tag{38}$$

where

$$\mathbf{S}_\alpha = -2\left(\frac{\alpha^2}{c'c''}\right)\hat{\mathbf{k}}''\hat{\mathbf{k}}'\,, \tag{39}$$

$$\mathbf{S}_\beta = 2\left(\frac{\beta^2}{c'c''}\right)[2\,\hat{\mathbf{k}}''\hat{\mathbf{k}}' - \hat{\mathbf{k}}'\hat{\mathbf{k}}'' - (\hat{\mathbf{k}}'\cdot\hat{\mathbf{k}}'')\mathbf{I}]\,, \tag{40}$$

$$\mathbf{S}_\rho = \mathbf{I} - \left(\frac{\alpha^2 - 2\beta^2}{c'c''}\right)\hat{\mathbf{k}}''\hat{\mathbf{k}}' - \left(\frac{\beta^2}{c'c''}\right)[\hat{\mathbf{k}}'\hat{\mathbf{k}}'' + (\hat{\mathbf{k}}'\cdot\hat{\mathbf{k}}'')\mathbf{I}]\,. \tag{41}$$

The prime and double prime in eqs (39)–(41) distinguish quantities evaluated along the incoming and outgoing ray paths at the scatterer $\mathbf{x}$, respectively. Two distinct generic wave speeds c' and c'' arise because of the possibility of *P*-to-*S* and *S*-to-*P* scattering at $\mathbf{x}$.

The wave vector and polarization notation associated with a source-to-scatterer-to-receiver path is summarized in Fig. 2. The incoming and outgoing wave speeds c', c'' and wave vectors $\hat{\mathbf{k}}'$, $\hat{\mathbf{k}}''$ are interchanged in the representations (39)–(41) in the case of a wave travelling along the reversed path from the

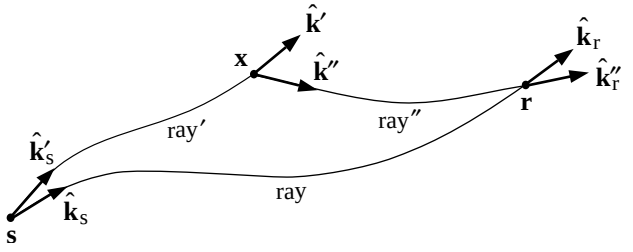

Figure 2. The Born approximation accounts for all singly scattered waves that propagate along a composite path ray′, ray″ from the source **s** to an arbitrary point heterogeneity **x**, and then to the receiver **r**. The take-off wave vectors along the unscattered and scattered paths at the source **s** are $\hat{\mathbf{k}}_s$ and $\hat{\mathbf{k}}_s'$, respectively; the incoming and outgoing wave vectors at the scatterer **x** are $\hat{\mathbf{k}}'$ and $\hat{\mathbf{k}}''$, respectively; the arrival wave vectors along the unscattered and scattered paths at the receiver **r** are $\hat{\mathbf{k}}_r$ and $\hat{\mathbf{k}}_r''$, respectively.

receiver **r** to the source **s**. The first-order perturbation to the Green tensor therefore satisfies the principle of source–receiver reciprocity, $\boldsymbol{\delta}\mathbf{G}_{sr} = \boldsymbol{\delta}\mathbf{G}_{rs}^{T}$.

The explicit factor of ω^2 in eq. (37) is a characteristic feature of Rayleigh scattering. High-frequency waves are scattered more strongly than low-frequency waves; the scattered power varies as ω^4. Scattered pulses in the time domain are twice-differentiated versions of the corresponding unscattered pulses; thus, contributions to $\boldsymbol{\delta}\mathbf{G}_{rs}(t)$ that have not passed through a caustic exhibit a $\pm\ddot{\delta}(t)$ time dependence, scattered waves that have passed through one caustic exhibit a $\pm\ddot{\delta}_H^{(1)}(t) = \mp(2/\pi)t^{-3}$ time dependence, and so on.

3.2 Perturbed seismogram

The first-order perturbation to the frequency-domain synchronous moment tensor response (20) is given by the obvious generalization of eq. (16):

$$\delta s(\omega) = \sqrt{2}M_0(i\omega)^{-1}\dot{m}(\omega)\hat{\mathbf{v}}\cdot[\hat{\mathbf{M}}:\nabla_s\boldsymbol{\delta}\mathbf{G}_{rs}^{T}(\omega)]\,. \tag{42}$$

We continue to use a prime and double prime to denote the source-to-scatterer and scatterer-to-receiver ray paths, respectively, and introduce the perturbed source and receiver factors analogous to (18)–(19):

$$\Lambda' = \sqrt{2}M_0(\rho_s c_s^5)^{-1/2}\,\hat{\mathbf{M}}:\frac{1}{2}\,(\hat{\mathbf{k}}_s'\hat{\mathbf{p}}_s' + \hat{\mathbf{p}}_s'\hat{\mathbf{k}}_s')\,, \tag{43}$$

$$\Upsilon'' = (\rho_r c_r)^{-1}(\hat{\mathbf{v}}\cdot\hat{\mathbf{p}}_r'')\,. \tag{44}$$

The perturbed frequency-domain response (42) can be written after some manipulation in the form

$$\delta s(\omega) = \left(\frac{\omega}{4\pi}\right)^2 \iiint_{\oplus}\left\{\sum_{\text{rays}'}\sum_{\text{rays}''}(c'c''^3)^{-1/2}\right.$$
$$\times\Lambda'\Upsilon''\Pi_{xs}\Pi_{rx}(\mathscr{R}_{xs}\mathscr{R}_{rx})^{-1}(\hat{\mathbf{p}}''\cdot\mathbf{S}\cdot\hat{\mathbf{p}}')\,\dot{m}(\omega)$$
$$\left.\times\exp i[-\omega(T_{xs}+T_{rx})+(M_{xs}+M_{rx})\pi/2]\right\}d^3\mathbf{x}\,. \tag{45}$$

The notation in (45) should, hopefully, be self-explanatory: Π_{xs} and Π_{rx} are the reflection–transmission coefficient products, $\mathscr{R}_{xs}$ and $\mathscr{R}_{rx}$ are the geometrical spreading factors, T_{xs} and T_{rx} are the traveltimes, and M_{xs} and M_{rx} are the Maslov indices along the primed source-to-scatterer and double-primed scatterer-to-receiver ray paths, respectively. The corresponding first-order perturbation to a seismogram in the time domain is

$$\delta s(t) = -\left(\frac{1}{4\pi}\right)^2 \iiint_{\oplus}\left\{\sum_{\text{rays}'}\sum_{\text{rays}''}(c'c''^3)^{-1/2}\right.$$
$$\times\Lambda'\Upsilon''\Pi_{xs}\Pi_{rx}(\mathscr{R}_{xs}\mathscr{R}_{rx})^{-1}(\hat{\mathbf{p}}''\cdot\mathbf{S}\cdot\hat{\mathbf{p}}')$$
$$\left.\times\dddot{m}_H^{(M_{xs}+M_{rx})}(t-T_{xs}-T_{rx})\right\}d^3\mathbf{x}\,, \tag{46}$$

where the triple dot denotes the third time derivative.

3.3 Abbreviated notation

It is convenient in what follows to rewrite the results (45) and (46) in terms of double-prime rays″ that are traced from the receiver **r** to the scatterer **x**, rather than *vice versa*. This is easily done using the obvious generalizations of the symmetries (10)–(11):

$$T_{rx} = T_{xr}\,, \qquad M_{rx} = M_{xr}\,, \tag{47}$$

$$\Pi_{rx} = \Pi_{xr}\,, \qquad c''\mathscr{R}_{rx} = c_r\mathscr{R}_{xr}\,. \tag{48}$$

At the same time, we shall introduce a new streamlined notation, which eliminates as many of the subscripts referring to **s**, **r** and **x** as possible. In this new notation, we distinguish quantities associated with the unperturbed ray, the forward source-to-scatterer ray′, and the backward receiver-to-scatterer ray″ by the presence of no prime, a single prime and a double prime, respectively:

$$T = T_{rs}\,, \qquad T' = T_{xs}\,, \qquad T'' = T_{xr}\,, \tag{49}$$

$$M = M_{rs}\,, \qquad M' = M_{xs}\,, \qquad M'' = M_{xr}\,, \tag{50}$$

$$\Pi = \Pi_{rs}\,, \qquad \Pi' = \Pi_{xs}\,, \qquad \Pi'' = \Pi_{xr}\,, \tag{51}$$

$$\mathscr{R} = \mathscr{R}_{rs}\,, \qquad \mathscr{R}' = \mathscr{R}_{xs}\,, \qquad \mathscr{R}'' = \mathscr{R}_{xr}\,. \tag{52}$$

The unperturbed frequency-domain response (20) and the time-domain seismogram (21) can then be written using no subscripts whatsoever in the form

$$s(\omega) = \frac{1}{4\pi}\sum_{\text{rays}}\Lambda\Upsilon\Pi\mathscr{R}^{-1}\dot{m}(\omega)\exp i(-\omega T + M\pi/2)\,, \tag{53}$$

$$s(t) = \frac{1}{4\pi}\sum_{\text{rays}}\Lambda\Upsilon\Pi\mathscr{R}^{-1}\dot{m}_H^{(M)}(t-T)\,. \tag{54}$$

The corresponding frequency-domain and time-domain perturbations (45)–(46) are

$$\delta s(\omega) = \left(\frac{\omega}{4\pi}\right)^2 \iiint_{\oplus}\left\{\sum_{\text{rays}'}\sum_{\text{rays}''}c_r^{-1}(c'c'')^{-1/2}\right.$$
$$\times\Lambda'\Upsilon''\Pi'\Pi''(\mathscr{R}'\mathscr{R}'')^{-1}(\hat{\mathbf{p}}''\cdot\mathbf{S}\cdot\hat{\mathbf{p}}')\,\dot{m}(\omega)$$
$$\left.\times\exp i[-\omega(T'+T'')+(M'+M'')\pi/2]\right\}d^3\mathbf{x}\,, \tag{55}$$

$$\delta s(t) = -\left(\frac{1}{4\pi}\right)^2 \iiint_{\oplus}\left\{\sum_{\text{rays}'}\sum_{\text{rays}''}c_r^{-1}(c'c'')^{-1/2}\right.$$
$$\times\Lambda'\Upsilon''\Pi'\Pi''(\mathscr{R}'\mathscr{R}'')^{-1}(\hat{\mathbf{p}}''\cdot\mathbf{S}\cdot\hat{\mathbf{p}}')$$
$$\left.\times\dddot{m}_H^{(M'+M'')}(t-T'-T'')\right\}d^3\mathbf{x}\,. \tag{56}$$

The double sums in eqs (55)–(56) are over *all possible* forward rays′ from the source **s** and backward rays″ from the receiver **r** to the scatterer **x**.

3.4 Rayleigh scattering coefficient

The quantity $\hat{\mathbf{p}}'' \cdot \mathbf{S} \cdot \hat{\mathbf{p}}'$ in eqs (55) and (56) is a dimensionless measure of the scattering strength of a wave with incoming polarization $\hat{\mathbf{p}}'$ into an outgoing wave with polarization $\hat{\mathbf{p}}''$ at the point **x**. We define three normalized *Rayleigh scattering coefficients*, one associated with each of the three types of volumetric heterogeneity $\delta\alpha$, $\delta\beta$, $\delta\rho$, by

$$\Omega_{\alpha,\beta,\rho} = -\frac{1}{2}\,(\hat{\mathbf{p}}'' \cdot \mathbf{S}_{\alpha,\beta,\rho} \cdot \hat{\mathbf{p}}')\,. \tag{57}$$

The coefficients $\Omega^{P\to P}_{\alpha,\beta,\rho}$, $\Omega^{S\to S}_{\alpha,\beta,\rho}$, $\Omega^{P\to S}_{\alpha,\beta,\rho}$ and $\Omega^{S\to P}_{\alpha,\beta,\rho}$ for both like-type and unlike-type scattering are summarized in Table 1; the polarization vectors of the incoming and outgoing *P* and *S* waves are denoted by $\hat{\mathbf{k}}'$, $\hat{\mathbf{k}}''$ and $\hat{\mathbf{q}}'$, $\hat{\mathbf{q}}''$, respectively. Recall that the *S*-wave polarization is degenerate, with two orthonormal possibilities $\hat{\mathbf{q}}_1$, $\hat{\mathbf{q}}_2$ for both $\hat{\mathbf{q}}'$ and $\hat{\mathbf{q}}''$. There are thus a total of 27 scattering coefficients in a spherical earth: *P*, *SV*, *SH*→*P*, *SV*, *SH* for each of $\delta\alpha$, $\delta\beta$, $\delta\rho$. Only *P*→*P* scattering off of a compressional wave heterogeneity is isotropic; the normalization factor $-1/2$ in the definition (57) has been

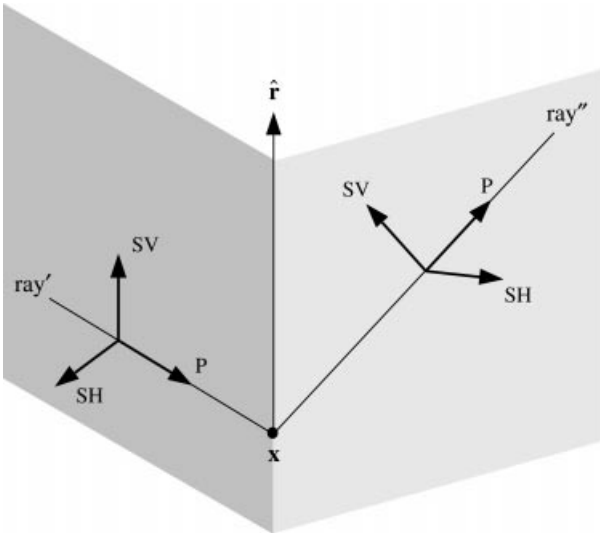

Figure 3. Geometrical convention used to plot the 27 absolute Rayleigh scattering coefficients in Fig. 4. The unit radial vector $\hat{\mathbf{r}}$ specifies the direction of the local vertical at the scatterer **x**; shading denotes the vertical planes containing the horizontal incoming ray′ and scattered outgoing ray″. The incoming and outgoing *SV* and *SH* polarizations are within and perpendicular to these planes, respectively.

Table 1. Normalized coefficient $\Omega_{\alpha,\beta,\rho}$ for Rayleigh scattering of a far-field body wave off a point heterogeneity $\delta\alpha$, $\delta\beta$, $\delta\rho$. The quantities $\hat{\mathbf{k}}'$, $\hat{\mathbf{k}}''$ and $\hat{\mathbf{q}}'$, $\hat{\mathbf{q}}''$ are the incoming and outgoing *P*-wave and *S*-wave polarizations, respectively.

P→*P* scattering:
$\Omega_\alpha = 1$
$\Omega_\beta = -2(\beta/\alpha)^2[1-(\hat{\mathbf{k}}'\cdot\hat{\mathbf{k}}'')^2]$
$\Omega_\rho = \frac{1}{2}(1-\hat{\mathbf{k}}'\cdot\hat{\mathbf{k}}'')-(\beta/\alpha)^2[1-(\hat{\mathbf{k}}'\cdot\hat{\mathbf{k}}'')^2]$
S→*S* scattering:
$\Omega_\alpha = 0$
$\Omega_\beta = (\hat{\mathbf{k}}'\cdot\hat{\mathbf{k}}'')(\hat{\mathbf{q}}'\cdot\hat{\mathbf{q}}'')+(\hat{\mathbf{k}}'\cdot\hat{\mathbf{q}}'')(\hat{\mathbf{k}}''\cdot\hat{\mathbf{q}}')$
$\Omega_\rho = \frac{1}{2}[-\hat{\mathbf{q}}'\cdot\hat{\mathbf{q}}''+(\hat{\mathbf{k}}'\cdot\hat{\mathbf{q}}'')(\hat{\mathbf{k}}''\cdot\hat{\mathbf{q}}')+(\hat{\mathbf{k}}'\cdot\hat{\mathbf{k}}'')(\hat{\mathbf{q}}'\cdot\hat{\mathbf{q}}'')]$
P→*S* scattering:
$\Omega_\alpha = 0$
$\Omega_\beta = 2(\beta/\alpha)(\hat{\mathbf{k}}'\cdot\hat{\mathbf{k}}'')(\hat{\mathbf{k}}'\cdot\hat{\mathbf{q}}'')$
$\Omega_\rho = -\frac{1}{2}(\hat{\mathbf{k}}'\cdot\hat{\mathbf{q}}'')+(\beta/\alpha)(\hat{\mathbf{k}}'\cdot\hat{\mathbf{k}}'')(\hat{\mathbf{k}}'\cdot\hat{\mathbf{q}}'')$
S→*P* scattering:
$\Omega_\alpha = 0$
$\Omega_\beta = 2(\beta/\alpha)(\hat{\mathbf{k}}''\cdot\hat{\mathbf{k}}')(\hat{\mathbf{k}}'\cdot\hat{\mathbf{q}}'')$
$\Omega_\rho = -\frac{1}{2}(\hat{\mathbf{k}}''\cdot\hat{\mathbf{q}}')+(\beta/\alpha)(\hat{\mathbf{k}}''\cdot\hat{\mathbf{k}}')(\hat{\mathbf{k}}''\cdot\hat{\mathbf{q}}')$

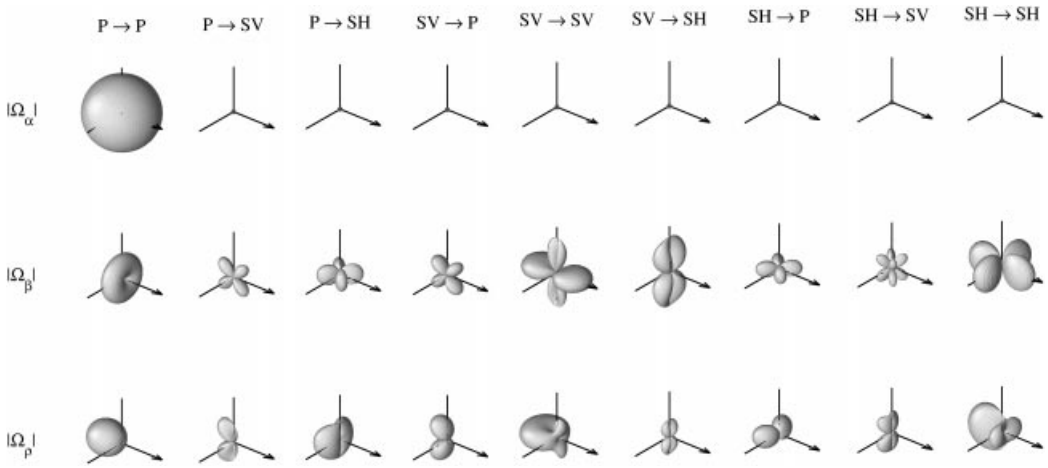

Figure 4. Perspective plots of the 27 possible absolute Rayleigh scattering coefficients $|\Omega^{P,SV,SH\to P,SV,SH}_{\alpha,\beta,\rho}|$ for the geometry shown in Fig. 3. The right-handed axes in each case are centred on the scatterer **x**, and aligned along the *P*, *SV*, *SH* polarizations of the incoming ray′; arrows denote the direction of the incident wave vector $\hat{\mathbf{k}}'$. The viewpoint makes it clear that the forward-scattering ($\hat{\mathbf{k}}'' = \hat{\mathbf{k}}'$) amplitude is zero, except for *P*→*P* scattering off a heterogeneity $\delta\alpha$ in *P*-wave speed, and *SV*→*SV* or *SH*→*SH* scattering off a heterogeneity $\delta\beta$ in *S*-wave speed. Each of these like-type forward-scattering processes has a normalized Rayleigh coefficient of unity: $\Omega^{P\to P}_\alpha = \Omega^{SV\to SV}_\beta = \Omega^{SH\to SH}_\beta = 1$.

introduced so that $\Omega_\alpha^{P\to P}=1$. We present a pictorial glossary of the 27 possible spherical earth scattering coefficients in Figs 3 and 4. The quantity plotted in each case is the absolute magnitude of the scattering strength, $|\Omega_{\alpha,\beta,\rho}^{P,SV,SH\to P,SV,SH}|$, for the particular case of a horizontally propagating incoming wave.

4 CROSS-CORRELATION TRAVELTIME MEASUREMENT

Luo & Schuster (1991) presented an explicit expression for the Fréchet derivative of a seismic traveltime measured by cross-correlation of an observed and a synthetic waveform. Unaware of this work, Marquering *et al.* (1999) derived an equivalent formula, and extended it to the case of a differential traveltime measured by cross-correlation of two observed waveforms. These results are briefly summarized here, in the interest of completeness. We regard α, β, ρ as an initial earth model, for which we are able to compute synthetic body wave seismograms $s(t)$, either by evaluating the JWKB ray-sum representation (54) or by some other method. Our objective is to relate an absolute or differential traveltime measurement to the unknown perturbations $\delta\alpha$, $\delta\beta$ and $\delta\rho$.

4.1 Absolute traveltime

Consider first the case of a single, well-isolated phase such as *P*, *PP*, *PcP* or *S*, *SS*, *ScS* that arrives during a time interval $t_1\le t\le t_2$. The cross-correlation of the synthetic and observed pulses is

$$\Gamma(\tau)=\int_{t_1}^{t_2} s(t-\tau)s^{\rm obs}(t)\,dt\,. \tag{58}$$

We assume that $s^{\rm obs}(t)$ can be adequately represented by a superposition of eqs (54) and (56):

$$s^{\rm obs}(t)=s(t)+\delta s(t)\,. \tag{59}$$

The cross-correlation (58) may in that case be written as a sum of a zeroth-order and a first-order term:

$$\Gamma(\tau)=\gamma(\tau)+\delta\gamma(\tau)\,, \tag{60}$$

where

$$\gamma(\tau)=\int_{t_1}^{t_2} s(t-\tau)s(t)\,dt\,, \tag{61}$$

$$\delta\gamma(\tau)=\int_{t_1}^{t_2} s(t-\tau)\delta s(t)\,dt\,. \tag{62}$$

In applications, the traveltime shift $\delta T=T^{\rm obs}-T$ of the observed phase $s^{\rm obs}(t)$ with respect to the synthetic $s(t)$ is determined by finding the maximum of $\Gamma(\tau)$. The unperturbed cross-correlation $\gamma(\tau)$ obviously attains its maximum at zero lag: $\partial_\tau\gamma(0)=0$. In the vicinity of this unperturbed maximum, we can expand (60) in a Taylor series, keeping terms of second order in the peak shift $\delta\tau$:

$$\begin{aligned}\Gamma(\delta\tau)&=\gamma(0)+\delta\tau\,\partial_\tau\gamma(0)+\frac{1}{2}\,\delta\tau^2\,\partial_{\tau\tau}\gamma(0)+\delta\gamma(0)+\delta\tau\,\partial_\tau\delta\gamma(0)\\&=\gamma(0)+\frac{1}{2}\,\delta\tau^2\,\partial_{\tau\tau}\gamma(0)+\delta\gamma(0)+\delta\tau\,\partial_\tau\delta\gamma(0)\,.\end{aligned} \tag{63}$$

To find the shift in the position of the maximum we differentiate (63) with respect to $\delta\tau$ and set the result equal to zero:

$$\partial_{\delta\tau}\left[\gamma(0)+\frac{1}{2}\,\delta\tau^2\,\partial_{\tau\tau}\gamma(0)+\delta\gamma(0)+\delta\tau\,\partial_\tau\delta\gamma(0)\right]=0\,, \tag{64}$$

or, equivalently,

$$\delta\tau=-\frac{\partial_\tau\delta\gamma(0)}{\partial_{\tau\tau}\gamma(0)}\,. \tag{65}$$

Upon carrying out the indicated operations in (65) and making the identification $\delta\tau=\delta T$, we obtain the final result

$$\delta T=\frac{\displaystyle\int_{t_1}^{t_2}\dot s(t)\,\delta s(t)\,dt}{\displaystyle\int_{t_1}^{t_2}\ddot s(t)s(t)\,dt}=\frac{\mathscr{R}e\displaystyle\int_0^\infty i\omega\,s^*(\omega)\,\delta s(\omega)\,d\omega}{\displaystyle\int_0^\infty\omega^2|s(\omega)|^2\,d\omega}\,, \tag{66}$$

where the asterisk denotes complex conjugation. We have assumed that $s(t)$ and $\delta s(t)$ both vanish outside the cross-correlation interval $t_1\le t\le t_2$, and used Parseval's equation to obtain the second equality. A *negative* traveltime shift, $\delta T<0$, corresponds to an *advance* in the arrival of the observed pulse $s^{\rm obs}(t)$ with respect to the synthetic pulse $s(t)$, whereas a *positive* traveltime shift, $\delta T>0$, corresponds to a *delay*.

4.2 Differential traveltime

The result (66) can be easily generalized to a shift in differential traveltime,

$$\Delta T=T_{\rm B}-T_{\rm A}\,, \tag{67}$$

measured by cross-correlation of two observed seismograms,

$$s_{\rm A}^{\rm obs}(t)=s_{\rm A}(t)+\delta s_{\rm A}(t)\quad\text{and}\quad s_{\rm B}^{\rm obs}(t)=s_{\rm B}(t)+\delta s_{\rm B}(t)\,.$$

The two signals A and B can either be the same phase, recorded at two closely spaced stations, or they can be two different phases, recorded at the same station. The cross-correlation

$$\Gamma(\tau)=\int_{t_1}^{t_2} s_{\rm A}^{\rm obs}(t-\tau)s_{\rm B}^{\rm obs}(t)\,dt \tag{68}$$

can again be decomposed into a zeroth-order and a first-order term:

$$\Gamma(\tau)=\gamma(\tau)+\delta\gamma(\tau)\,, \tag{69}$$

where

$$\gamma(\tau)=\int_{t_1}^{t_2} s_{\rm A}(t-\tau)s_{\rm B}(t)\,dt\,, \tag{70}$$

$$\delta\gamma(\tau)=\int_{t_1}^{t_2}\left[s_{\rm A}(t-\tau)\,\delta s_{\rm B}(t)+\delta s_{\rm A}(t-\tau)s_{\rm B}(t)\right]dt\,. \tag{71}$$

The unperturbed cross-correlation in this case attains its maximum at the differential traveltime (67) between the two phases A and B in the spherical earth model. The perturbations $\delta\alpha$, $\delta\beta$, $\delta\rho$ shift the position τ of this maximum by an amount $\delta\tau=\delta(\Delta T)$. The Taylor series expansion of (69) about the spherical earth maximum is

$$\begin{aligned}\Gamma(\tau+\delta\tau)&=\gamma(\tau)+\delta\tau\,\partial_\tau\gamma(\tau)+\frac{1}{2}\,\delta\tau^2\,\partial_{\tau\tau}\gamma(\tau)+\delta\gamma(\tau)+\delta\tau\,\partial_\tau\delta\gamma(\tau)\\&=\gamma(\tau)+\frac{1}{2}\,\delta\tau^2\,\partial_{\tau\tau}\gamma(\tau)+\delta\gamma(\tau)+\delta\tau\,\partial_\tau\delta\gamma(\tau)\,,\end{aligned} \tag{72}$$

where we have once again used the unperturbed condition $\partial_\tau\gamma(\tau)=0$ to obtain the second equality. The shift in the maximum is obtained from the perturbed condition

$$\partial_{\delta\tau}\left[\gamma(\tau)+\frac{1}{2}\,\delta\tau^2\,\partial_{\tau\tau}\gamma(\tau)+\delta\gamma(\tau)+\delta\tau\,\partial_\tau\delta\gamma(\tau)\right]=0\,. \tag{73}$$

This leads to a result identical to (65), with the argument zero replaced by the unperturbed lag τ:

$$\delta\tau=-\frac{\partial_\tau\delta\gamma(\tau)}{\partial_{\tau\tau}\gamma(\tau)}\,. \tag{74}$$

Upon making the identifications $\tau=\Delta T$ and $\delta\tau=\delta(\Delta T)$, we find that

$$\begin{aligned}\delta(\Delta T)&=\frac{\displaystyle\int_{t_1}^{t_2}[\dot s_{\rm A}(t-\Delta T)\,\delta s_{\rm B}(t)+\delta\dot s_{\rm A}(t-\Delta T)s_{\rm B}(t)]\,dt}{\displaystyle\int_{t_1}^{t_2}\ddot s_{\rm A}(t-\Delta T)s_{\rm B}(t)\,dt}\\&=\frac{\mathscr{R}e\displaystyle\int_0^\infty i\omega[s_{\rm A}^*(\omega)\,\delta s_{\rm B}(\omega)+\delta s_{\rm A}^*(\omega)\,s_{\rm B}(\omega)]\,e^{i\omega\Delta T}\,d\omega}{\mathscr{R}e\displaystyle\int_0^\infty\omega^2 s_{\rm A}^*(\omega)\,s_{\rm B}(\omega)\,e^{i\omega\Delta T}\,d\omega}\,,\end{aligned} \tag{75}$$

where the asterisks again denote complex conjugation in the frequency domain.

5 TRAVELTIME FRÉCHET KERNEL

Determination of the first-order dependence of an absolute or differential traveltime measurement upon the perturbations $\delta\alpha$, $\delta\beta$, $\delta\rho$ is now a straightforward matter—we simply employ the JWKB representations (53) and (55) in eqs (66) and (75), and interchange the order of integration.

5.1 Single-phase kernel

In the case of an absolute traveltime δT, we regard $s(\omega)$ as a single phase, that is, a single ray in the representation (53). We retain the double summation over source-to-scatterer rays′ and receiver-to-scatterer rays″ in (55) to guarantee the inclusion of all possible scattered waves that may arrive during the time interval of interest, $t_1\le t\le t_2$. Note that the concatenation of rays′ and rays″ need not be of the same 'type' as the central ray; for example, scattered waves that never experience a surface reflection may arrive in the same time window as a *PP* or *SS* wave, and thus contribute to the cross-correlation traveltime shift δT, as illustrated in Fig. 5.

It is convenient to define the dimensionless product of ratios

$$\begin{aligned}N&=\left(\frac{\Lambda'}{\Lambda}\right)\left(\frac{\Upsilon''}{\Upsilon}\right)\left(\frac{\Pi'\Pi''}{\Pi}\right)\\&=\left[\frac{\hat{\mathbf{M}}\colon\frac{1}{2}\,(\hat{\mathbf{k}}_{\rm s}'\hat{\mathbf{p}}_{\rm s}'+\hat{\mathbf{p}}_{\rm s}'\hat{\mathbf{k}}_{\rm s}')}{\hat{\mathbf{M}}\colon\frac{1}{2}\,(\hat{\mathbf{k}}_{\rm s}\hat{\mathbf{p}}_{\rm s}+\hat{\mathbf{p}}_{\rm s}\hat{\mathbf{k}}_{\rm s})}\right]\left(\frac{\hat{\boldsymbol{\nu}}\cdot\hat{\mathbf{p}}_{\rm r}''}{\hat{\boldsymbol{\nu}}\cdot\hat{\mathbf{p}}_{\rm r}}\right)\left(\frac{\Pi_{\rm xs}\Pi_{\rm xr}}{\Pi_{\rm rs}}\right).\end{aligned} \tag{76}$$

The traveltime perturbation δT can be written in the form

$$\delta T=\iiint_\oplus\left[K_\alpha\left(\frac{\delta\alpha}{\alpha}\right)+K_\beta\left(\frac{\delta\beta}{\beta}\right)+K_\rho\left(\frac{\delta\rho}{\rho}\right)\right]d^3\mathbf{x}\,, \tag{77}$$

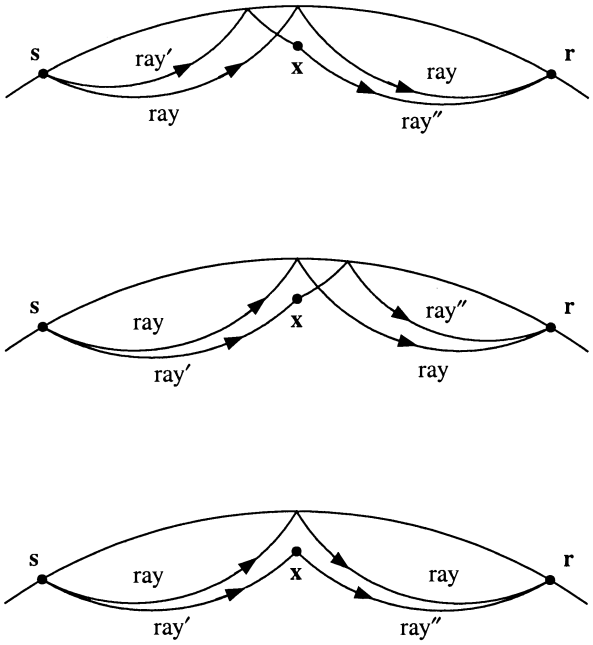

Figure 5. A 'like-type' scattering path is one that has the same number and type of boundary interactions as the unperturbed ray path, whereas an 'unlike-type' scattering path is one that does not. Both 'types' of scattering paths must be included in evaluating the double sum (78) over rays′, rays″. In this example, the unperturbed ray path is that of a *PP* or *SS* wave, with a single underside reflection off the free surface. (Top and middle) Two 'like-type' scattering paths, with one surface reflection each, along the ray′ from the source **s** to the scatterer **x**, and along the ray″ from the scatterer to the receiver **r**, respectively. (Bottom) An 'unlike-type' scattering path, with no free-surface reflections. The traveltime $T'+T''$ along all three of these paths can be very near the unperturbed traveltime T; for this reason, they can contribute significantly to the Fréchet kernel K.

where

$$\begin{aligned}K_{\alpha,\beta,\rho}=&-\frac{1}{2\pi}\sum_{\rm rays'}\sum_{\rm rays''}N\Omega_{\alpha,\beta,\rho}\left(\frac{1}{\sqrt{c'c''}}\right)\left(\frac{\mathscr{R}}{c_{\rm r}\mathscr{R}'\mathscr{R}''}\right)\\&\times\frac{\displaystyle\int_0^\infty\omega^3|\dot m(\omega)|^2\sin[\omega(T'+T''-T)-(M'+M''-M)\pi/2]\,d\omega}{\displaystyle\int_0^\infty\omega^2|\dot m(\omega)|^2\,d\omega}\,.\end{aligned} \tag{78}$$

The three amigos K_α, K_β, K_ρ in eq. (77) are the *3-D Fréchet kernels* relating the observable δT to the fractional perturbations $\delta\alpha/\alpha$, $\delta\beta/\beta$, $\delta\rho/\rho$ in compressional wave speed, shear wave speed and density. Eq. (78) provides an explicit representation of these kernels as a sum over forward rays′ and backward rays″.

The power spectrum $|\dot m(\omega)|^2$ of the source time function specifies the frequency content of the cross-correlated arrivals. This serves as a reminder that K_α, K_β, K_ρ are the Fréchet kernels of a *finite-frequency* traveltime measurement δT. If the synthetic and observed seismograms, $s(t)$ and $s^{\rm obs}(t)$, are bandpass filtered prior to cross-correlation, the power spectrum will be altered, $|\dot m(\omega)|^2\to|\dot m(\omega)|^2_{\rm filtered}$, and the kernels K_α, K_β, K_ρ will all change. The common factor $\sin[\omega(T'+T''-T)-(M'+M''-M)\pi/2]$ is identically

equal to zero at every scattering point **x** along a least-time ($M_1 = M_2 = 0$) geometrical ray; this provides an immediate explanation of the banana–doughnut character of a direct *P*-wave or *S*-wave kernel. We shall elaborate upon this explanation and also show how (78) explains the more complicated geometry of a minimax *PP* or *SS* kernel in Banana–Doughnut II.

5.2 Differential kernel

To obtain the Fréchet kernel for a differential traveltime measurement $\delta(\Delta T) = \delta(T_B - T_A)$, we model each of the phases $s_A(\omega)$ and $s_B(\omega)$ as a single ray in (53), with associated amplitude pre-factors $\Lambda_A \Upsilon_A \Pi_A$ and $\Lambda_B \Upsilon_B \Pi_B$, geometrical spreading factors $\mathscr{R}_A$ and $\mathscr{R}_B$, and traveltimes T_A and T_B. The ratio of integrals (75) reduces to its simplest form in the special case that the Maslov indices of the phases A and B are identical, so that the two cross-correlated pulses have the same shape:

$$M_A = M_B \Rightarrow \dot{m}_H^{(M_A)}(t) = \dot{m}_H^{(M_B)}(t) \,. \tag{79}$$

In practice, this is the only case of interest; in fact, any inequality $M_A \neq M_B$ in the number of caustic phase shifts is commonly rectified by processing, for example, by Hilbert transformation of *P* or *S* prior to cross-correlation with the minimax phases *PP* or *SS* (Kuo *et al.* 1987; Sheehan & Solomon 1991; Woodward & Masters 1991). The perturbations $\delta s_A(\omega)$ and $\delta s_B(\omega)$ are considered to be *identical* double sums (55) over all possible rays′ and rays″: $\delta s_A(\omega) = \delta s_B(\omega) = \delta s(\omega)$. With these assumptions, we find that the differential traveltime perturbation (75) can be written in a manner analogous to (77), namely,

$$\delta(\Delta T) = \iiint_{\oplus} \left[K_\alpha \left(\frac{\delta\alpha}{\alpha} \right) + K_\beta \left(\frac{\delta\beta}{\beta} \right) + K_\rho \left(\frac{\delta\rho}{\rho} \right) \right] d^3\mathbf{x} \,. \tag{80}$$

The pre-factors $\Lambda_A \Upsilon_A \Pi_A$, $\Lambda_B \Upsilon_B \Pi_B$, spreading factors $\mathscr{R}_A$, $\mathscr{R}_B$ and exponentials $\exp(-i\omega T_A)$, $\exp(-i\omega T_B)$, $\exp(i\omega \Delta T)$ conspire so that the kernels in (80) reduce to

$$K^{B-A}_{\alpha,\beta,\rho} = K^B_{\alpha,\beta,\rho} - K^A_{\alpha,\beta,\rho} \quad \text{if} \quad M_A = M_B \,. \tag{81}$$

The result (81) has an elegant physical interpretation: every Fréchet kernel $K^{B-A}_{\alpha,\beta,\rho}$ for an 'identical pulse shape' differential traveltime measurement, $\delta(\Delta T) = \delta(T_B - T_A)$, is simply the *difference of the individual Fréchet kernels*, $K^B_{\alpha,\beta,\rho} - K^A_{\alpha,\beta,\rho}$. Strictly speaking, the implication (79) is valid only in a perfectly elastic earth; if there is a substantial difference in the attenuation times of the two phases, $T^*_A \neq T^*_B$, it may be necessary to apply an attenuation equalization, as well as a Hilbert transformation, to either phase A or phase B prior to cross-correlation.

5.3 Summary of computational procedure

Let us summarize the steps needed to compute a single-phase Fréchet kernel $K_{\alpha,\beta,\rho}$.

(1) Trace the geometrical ray corresponding to the phase of interest from the source **s** to the receiver **r**.

(2) Compute the traveltime T, the Maslov index M, the reflection–transmission product Π, the geometrical spreading factor $\mathscr{R}$, and the source and receiver factors Λ and Υ along this central ray.

(3) Trace all possible forward rays′ from the source **s** and all possible backward rays″ from the receiver **r** to every scatterer **x** in $\oplus$.

(4) Compute the traveltimes T', T'', the Maslov indices M', M'', the reflection–transmission products Π', Π'', the geometrical spreading factors $\mathscr{R}'$, $\mathscr{R}''$, the source and receiver factors Λ', Υ'', and the scattering cross-sections $\Omega_{\alpha,\beta,\rho}$ along each of these scattered rays′, rays″.

(5) Finally, evaluate the double sum (78).

The need to trace *all possible* rays′ from the source **s** and rays″ from the receiver **r** to *every* scatterer **x** in $\oplus$ makes this procedure computationally intensive.

5.4 Validity

Two distinct approximations are embodied in the results (77)–(78) and (80)–(81). First, we have systematically linearized the dependence of an absolute or differential cross-correlation traveltime shift δT, $\delta(\Delta T)$ upon the model perturbations $\delta\alpha$, $\delta\beta$, $\delta\rho$. Such a linearization is appropriate, since our objective is to compute the first-order Fréchet derivatives $\partial T/\partial\alpha$, $\partial T/\partial\beta$, $\partial T/\partial\rho$ and $\partial(\Delta T)/\partial\alpha$, $\partial(\Delta T)/\partial\beta$, $\partial(\Delta T)/\partial\rho$. If we were able to use the *exact* unperturbed Green tensors $\mathbf{G}_{rx}$ and $\mathbf{G}_{xs}$ to compute the perturbed Green tensor $\boldsymbol{\delta}\mathbf{G}_{rs}$ in eq. (36), then (66) and (75) would yield the *exact* Fréchet derivatives. It follows that the results (78) and (81) fail to give the exact Fréchet kernels $K_{\alpha,\beta,\rho}$ only as a result of our second approximation—the use of a ray-theoretical representation (8) of $\mathbf{G}_{rx}$ and $\mathbf{G}_{xs}$ in (36).

The conditions guaranteeing the validity of such a ray-theoretical representation of the response are well known—the unperturbed parameters α, β, ρ must be smooth everywhere in $\oplus$, except at the internal discontinuities Σ_{SS} and Σ_{FS} (Červený *et al.* 1977; Červený & Hron 1980; Červený 1985; Kravstov & Orlov 1990; Dahlen & Tromp 1998, Sections 15.1 and 5.2). Core-grazing rays and other source–receiver paths for which ray theory is known to fail must be avoided; with that proviso, the results (78) and (81) should provide an accurate representation of the Fréchet kernels $K_{\alpha,\beta,\rho}$ everywhere within a piecewise-smooth earth model α, β, ρ. If another numerical method such as normal-mode or surface wave summation has been used to synthesize the seismogram $s(t)$, which is cross-correlated with $s^{obs}(t)$, it may be prudent to verify that the waveform is in reasonable agreement with ray theory.

The remarks in the previous paragraph only address the issue of the accuracy of the ray-theoretical representation of the Fréchet kernels (78) and (81). There remains the question of the accuracy of the first-order relationships (77) and (80) expressing an absolute or differential traveltime measurement δT or $\delta(\Delta T)$ in terms of these Fréchet kernels. This is, in a sense, a familiar question, since it arises whenever a geophysical inverse problem is linearized. As usual in applications of the Born approximation, the perturbations $\delta\alpha$, $\delta\beta$, $\delta\rho$ may be arbitrarily rough throughout the earth model $\oplus$, provided they are sufficiently slight:

$$|\delta\alpha| \ll \alpha \,, \qquad |\delta\beta| \ll \beta \,, \qquad |\delta\rho| \ll \rho \,. \tag{82}$$

The precise meaning of the symbol $\ll$ in (82) is a complicated issue, which depends upon the frequency and wavelength of the dominant waves in the pulses $s(t)$ and $s^{obs}(t)$, the characteristic scale length of the 3-D heterogeneity $\delta\alpha$, $\delta\beta$, $\delta\rho$, and

the propagation distance between the source **s** and receiver **r**. In practice, measured traveltime shifts δT and $\delta(\Delta T)$ will be well described by the local linearized relations (77) and (80) only if they are small compared to the dominant period of the cross-correlated waves. Longer traveltime shifts, cycle skips and significant pulse distortions due to heterogeneity-induced multipathing cannot be modelled using the Born approximation.

6 PARAXIAL APPROXIMATION

In this section, we describe an approximate procedure for computing $K_{\alpha,\beta,\rho}$, which eliminates the need to conduct repeated two-point ray tracing. This approximation is motivated by the observation that the traveltime shift δT is generally sensitive only to the perturbations $\delta\alpha$, $\delta\beta$, $\delta\rho$ in a relatively slender hollow banana surrounding the central geometrical ray. A rough rule of thumb is that $K_{\alpha,\beta,\rho}\approx 0$ at any scatterer **x** that is not within the first Fresnel zone, defined by

$$0\le\bar{\omega}(T'+T''-T)\le\pi\,, \tag{83}$$

where $\bar{\omega}$ is the dominant frequency in the power spectrum $|\dot{m}(\omega)|^2$ of the cross-correlated pulse. Whenever the traveltime difference $T'+T''-T$ is significantly greater than that given by (83), the magnitude of the kernel $K_{\alpha,\beta,\rho}$ is diminished by destructive interference of adjacent frequencies ω and $\omega+d\omega$ in the integral (78). To obtain an approximate kernel, we systematically exploit this confinement of the strong sensitivity of δT to the immediate vicinity of the central ray.

6.1 Forward scattering

We ignore all source-to-scatterer-to-receiver paths that are not of the same 'type' as the unperturbed path; it is conventional to refer to the 'like-type' scattering paths in the vicinity of the central ray as *paraxial rays*. We begin by noting that the initial and final wave vector and polarization on such a paraxial ray path are, to a first approximation, identical to those on the central ray path; that is, $\hat{\mathbf{k}}'_{\rm s}=\hat{\mathbf{k}}_{\rm s}$, $\hat{\mathbf{p}}'_{\rm s}=\hat{\mathbf{p}}_{\rm s}$ and $\hat{\mathbf{k}}''_{\rm r}=\hat{\mathbf{k}}_{\rm r}$, $\hat{\mathbf{p}}''_{\rm r}=\hat{\mathbf{p}}_{\rm r}$ at the source **s** and the receiver **r**, respectively. Waves travelling along the two paths experience very nearly the same boundary interactions, so that, to the same approximation, $\Pi_{\rm xs}\Pi_{\rm xr}=\Pi_{\rm rs}$. Combining these results, we find that the pre-factor (76) reduces to

$$N=1\,. \tag{84}$$

The outgoing and incoming wave vectors at the scatterer **x** are likewise nearly identical: $\hat{\mathbf{k}}''=\hat{\mathbf{k}}'$. The outgoing shear wave polarization may be chosen arbitrarily; we specify that $\hat{\mathbf{q}}''=\hat{\mathbf{q}}'$. Upon examining the formulae in Table 1, we find that only $P\to P$ scattering off a compressional wave-speed heterogeneity $\delta\alpha$ and like-type $S\to S$ scattering off a shear wave-speed heterogeneity $\delta\beta$ are significant in this *forward-scattering approximation*. Furthermore, the normalized amplitude of each of these forward-scattering processes is unity:

$$\Omega_\alpha^{P\to P}=\Omega_\beta^{SV\to SV}=\Omega_\beta^{SH\to SH}=1\,, \tag{85}$$

$$\text{all other } \Omega_{\alpha,\beta,\rho}^{P,SV,SH\to P,SV,SH}=0\,. \tag{86}$$

The results (85)–(86) may also be verified by visual inspection of Fig. 4.

6.2 Ray-centred coordinates

It is convenient in the paraxial approximation to express the position of every scatterer in the form

$$\mathbf{x}=\boldsymbol{\xi}+\mathbf{q}\,, \tag{87}$$

where $\boldsymbol{\xi}$ is the nearest point on the central ray path, as illustrated in Fig. 6. The difference vector satisfies $\hat{\mathbf{k}}\cdot\mathbf{q}=0$, where $\hat{\mathbf{k}}$ is the unit wave vector at $\boldsymbol{\xi}$. Points $\mathbf{s}\le\boldsymbol{\xi}\le\mathbf{r}$ along the central ray can be parametrized by the arclength $0\le l\le L$, where the endpoints $l=0$ and $l=L$ correspond to the source **s** and receiver **r**, respectively. Upon decomposing **q** into two orthogonal components, $\mathbf{q}=q_1\hat{\mathbf{q}}_1+q_2\hat{\mathbf{q}}_2$, we can represent every scatterer **x** in terms of the so-called *ray-centred coordinates* (Červený & Hron 1980; Červený 1985):

$$\mathbf{x}=(q_1,\,q_2,\,l)\,. \tag{88}$$

In a spherically symmetric earth, we choose $\hat{\mathbf{q}}_1=\hat{\mathbf{q}}_{SV}$ and $\hat{\mathbf{q}}_2=\hat{\mathbf{q}}_{SH}$, as already noted. In that case, q_1 and q_2 are measured within and perpendicular to the central ray plane, respectively. The ratio of geometrical spreading factors in the first line of eq. (78) can be approximated by the corresponding ratio on the central ray:

$$\frac{\mathscr{R}_{\rm rs}}{c_{\rm r}\mathscr{R}_{\rm xs}\mathscr{R}_{\rm xr}}=\frac{\mathscr{R}_{\rm rs}}{c_{\rm r}\mathscr{R}_{\xi\rm s}\mathscr{R}_{\xi\rm r}}\,, \tag{89}$$

where we have reverted to our original subscript-laden notation for clarity.

6.3 Traveltime difference

Turning next to the phase factors in the argument of the oscillatory term $\sin[\omega(T_{\rm xs}+T_{\rm xr}-T_{\rm rs})-(M_{\rm xs}+M_{\rm xr}-M_{\rm rs})\pi/2]$, we replace the Maslov indices by their values on the central ray:

$$M_{\rm xs}=M_{\xi\rm s}\,,\qquad M_{\rm xr}=M_{\xi\rm r}\,. \tag{90}$$

The only deviation of the paraxial from the central ray that is accounted for is the difference in traveltime. The resulting approximation is self-consistent, since $T_{\rm xs}+T_{\rm xr}-T_{\rm rs}$ is multiplied by the frequency ω, and we are interested in the high-frequency limit, $\omega\to\infty$. Following Červený & Hron (1980) and Červený (1985), we approximate the paraxial time difference by a quadratic:

$$T_{\rm xs}+T_{\rm xr}-T_{\rm rs}=\frac{1}{2}\,\mathbf{q}^{\rm T}\cdot(\mathbf{M}_{\xi\rm s}+\mathbf{M}_{\xi\rm r})\cdot\mathbf{q}\,. \tag{91}$$

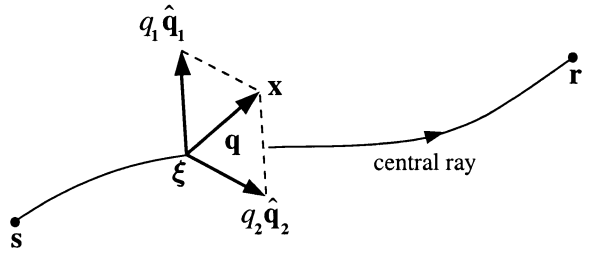

Figure 6. Perpendicular projection of a scatterer **x** onto the paraxial point $\boldsymbol{\xi}$, situated on the central geometrical ray from the source **s** to the receiver **r**. The off-path difference vector is expressed in terms of the two orthogonal shear wave polarizations: $\mathbf{q}=q_1\hat{\mathbf{q}}_1+q_2\hat{\mathbf{q}}_2$. The ray-centred coordinates of the scatterer are $\mathbf{x}=(q_1,\,q_2,\,l)$, where l is the arclength along the central ray.

There is no term linear in the off-path vector $\mathbf{q}$ by virtue of the stationarity of the traveltime along the central ray. The quantities $\mathbf{M}_{\xi s}$ and $\mathbf{M}_{\xi r}$ are the 2×2 *Hessian matrices*, whose entries are the second partial derivatives $\partial^2 T/\partial q_i \partial q_j$ of the traveltime field at the point $\boldsymbol{\xi}$, measured from the source $\mathbf{s}$ and the receiver $\mathbf{r}$, respectively.

6.4 Properties of the Hessian

The eigenvalues of the matrices $c\mathbf{M}_{\xi s}$ and $c\mathbf{M}_{\xi r}$ are the principal curvatures of the forward- and backward-propagating wave fronts emanating from $\mathbf{s}$ and $\mathbf{r}$. Since wave-front curvature is a manifestation of geometrical spreading, it is not surprising that there is an intimate relation between the spreading factors $\mathscr{R}_{\xi s}$, $\mathscr{R}_{\xi r}$ and the Hessians $\mathbf{M}_{\xi s}$, $\mathbf{M}_{\xi r}$. We adapt an argument by Snieder & Chapman (1998) to obtain this relation in the present section.

Červený & Hron (1980) and Červený (1985) show that the source and receiver Hessians satisfy a pair of forward and backward Ricatti equations:

$$\frac{d\mathbf{M}_{\xi s}}{dl} + c\mathbf{M}_{\xi s}^2 + c^{-1}\mathbf{V}_\xi = \mathbf{0}\,, \tag{92}$$

$$\frac{d\mathbf{M}_{\xi r}}{dl} - c\mathbf{M}_{\xi r}^2 - c^{-1}\mathbf{V}_\xi = \mathbf{0}\,. \tag{93}$$

The quantity $\mathbf{V}_\xi$ is the 2×2 matrix of second partial derivatives $\partial^2 c/\partial q_i \partial q_j$ of the wave speed at the point $\mathbf{s}\le\boldsymbol{\xi}\le\mathbf{r}$ along the central ray. The two eqs (92)–(93) can be combined to obtain

$$\frac{d}{dl}\det(\mathbf{M}_{\xi s}+\mathbf{M}_{\xi r}) + c\,\mathrm{tr}\,(\mathbf{M}_{\xi s}-\mathbf{M}_{\xi r})\det(\mathbf{M}_{\xi s}+\mathbf{M}_{\xi r}) = 0\,, \tag{94}$$

where det and tr denote the determinant and trace, respectively. Since eq. (94) is independent of the wave-speed derivatives $\mathbf{V}_\xi$, it can be integrated analytically,

$$[\ln\det(\mathbf{M}_{\xi s}+\mathbf{M}_{\xi r})]_{l'}^{l''} = -\int_{l'}^{l''} c(\mathrm{tr}\,\mathbf{M}_{\xi s} - \mathrm{tr}\,\mathbf{M}_{\xi r})\,dl\,, \tag{95}$$

at any two points $\mathbf{s}\le\boldsymbol{\xi}'\le\boldsymbol{\xi}''\le\mathbf{r}$ at consecutive distances $0\le l'\le l''\le L$ along the ray. The geometrical spreading factors $\mathscr{R}_{\xi s}$ and $\mathscr{R}_{\xi r}$ likewise satisfy a pair of forward and backward differential equations (Červený & Hron 1980; Červený 1985):

$$\frac{d\mathscr{R}_{\xi s}}{dl} = \frac{1}{2}\,c(\mathrm{tr}\,\mathbf{M}_{\xi s})\mathscr{R}_{\xi s}\,, \tag{96}$$

$$\frac{d\mathscr{R}_{\xi r}}{dl} = -\frac{1}{2}\,c(\mathrm{tr}\,\mathbf{M}_{\xi r})\mathscr{R}_{\xi r}\,. \tag{97}$$

Upon integrating these relations and adding, we obtain

$$[\ln(\mathscr{R}_{\xi s}\mathscr{R}_{\xi r})^2]_{l'}^{l''} = \int_{l'}^{l''} c(\mathrm{tr}\,\mathbf{M}_{\xi s} - \mathrm{tr}\,\mathbf{M}_{\xi r})\,dl\,. \tag{98}$$

The right sides of eqs (95) and (98) are identical except for the sign; hence,

$$[\ln(\mathscr{R}_{\xi s}\mathscr{R}_{\xi r})^2]_{l'}^{l''} = [\ln\det(\mathbf{M}_{\xi s}+\mathbf{M}_{\xi r})]_{l''}^{l'}\,, \tag{99}$$

or, equivalently,

$$\frac{\mathscr{R}_{\xi'' s}\mathscr{R}_{\xi'' r}}{\mathscr{R}_{\xi' s}\mathscr{R}_{\xi' r}} = \left|\frac{\det(\mathbf{M}_{\xi' s}+\mathbf{M}_{\xi' r})}{\det(\mathbf{M}_{\xi'' s}+\mathbf{M}_{\xi'' r})}\right|^{1/2} \tag{100}$$

for any two points $\mathbf{s}\le\boldsymbol{\xi}'\le\boldsymbol{\xi}''\le\mathbf{r}$. The proportionality relation (100) stipulates that the two quantities $\mathscr{R}_{\xi s}\mathscr{R}_{\xi r}$ and $|\det(\mathbf{M}_{\xi s}+\mathbf{M}_{\xi r})|^{1/2}$ vary inversely along a ray:

$$\frac{1}{\mathscr{R}_{\xi s}\mathscr{R}_{\xi r}} = \text{constant}\times\sqrt{|\det(\mathbf{M}_{\xi s}+\mathbf{M}_{\xi r})|}\,. \tag{101}$$

The limiting values of the spreading factors $\mathscr{R}_{\xi s}$, $\mathscr{R}_{\xi r}$ and the determinants $\det\mathbf{M}_{\xi s}$, $\det\mathbf{M}_{\xi r}$ at the endpoints $\boldsymbol{\xi}\to\mathbf{s}$ and $\boldsymbol{\xi}\to\mathbf{r}$ are

$$\mathscr{R}_{\xi s}\to l \text{ and } \det\mathbf{M}_{\xi s}\to c_s^{-2}l^{-2} \text{ as } l\to 0\,, \tag{102}$$

$$\mathscr{R}_{\xi r}\to L-l \text{ and } \det\mathbf{M}_{\xi r}\to c_r^{-2}(L-l)^{-2} \text{ as } l\to L\,. \tag{103}$$

Upon using (102)–(103) together with the spreading-factor symmetry $c_s\mathscr{R}_{rs} = c_r\mathscr{R}_{sr}$ to evaluate the constant in eq. (101), we obtain the desired relation:

$$\frac{\mathscr{R}_{rs}}{c_r\mathscr{R}_{\xi s}\mathscr{R}_{\xi r}} = \sqrt{|\det(\mathbf{M}_{\xi s}+\mathbf{M}_{\xi r})|}\,. \tag{104}$$

All four of the quantities $\mathbf{M}_{\xi s}$, $\mathbf{M}_{\xi r}$ and $\mathscr{R}_{\xi s}$, $\mathscr{R}_{\xi r}$ can exhibit jump discontinuities at the boundaries Σ; the jumps in the left and right sides of (104) are, however, always identical, so that the equality remains valid regardless of the number of reflections, transmissions or conversions along a ray.

There is also a relation between the Maslov index difference $M_{\xi s}+M_{\xi r}-M_{rs}$ and the *signature*, or number of positive eigenvalues minus the number of negative eigenvalues, of the matrix $\mathbf{M}_{\xi s}+\mathbf{M}_{\xi r}$. Since $M_{\xi s}+M_{\xi r}-M_{rs}$ changes by 1, whereas $\mathrm{sig}\,(\mathbf{M}_{\xi s}+\mathbf{M}_{\xi r})$ changes by 2 upon every passage through a caustic, and since the limiting values of these quantities at the two endpoints $\boldsymbol{\xi}\to\mathbf{s}$ and $\boldsymbol{\xi}\to\mathbf{r}$ are zero and 2, respectively, we must have

$$M_{\xi s}+M_{\xi r}-M_{rs} = \frac{1}{2}\,[\mathrm{sig}\,(\mathbf{M}_{\xi s}+\mathbf{M}_{\xi r})-2]\,. \tag{105}$$

Eq. (105) is also valid regardless of the number or type of boundary interactions experienced by a wave.

6.5 Paraxial kernel

Eqs (84)–(86), (89)–(91) and (104)–(105) constitute all of the ingredients needed to compute the traveltime Fréchet kernel (78) in the paraxial approximation. Once again, we shall express the result using a streamlined notation, in which the subscripts referring to $\mathbf{s}$, $\mathbf{r}$ and $\boldsymbol{\xi}$ are eliminated. Specifically, we now identify the forward and backward paths *along the central ray* by a prime and a double prime, respectively, writing

$$\mathbf{M}' = \mathbf{M}_{\xi s}\,, \qquad \mathbf{M}'' = \mathbf{M}_{\xi r}\,. \tag{106}$$

The forward-scattering conditions (85)–(86) stipulate that a traveltime perturbation in the paraxial approximation is sensitive *only to the speed of the propagating waves*; that is, the threefold dependence upon $\delta\alpha$, $\delta\beta$ and $\delta\rho$ in (77) is replaced by

$$\delta T = \iiint_{\oplus} K(\delta c/c)\,d^3\mathbf{x}. \tag{107}$$

The Fréchet kernel $K(\mathbf{x}) = K(q_1, q_2, l)$ in (107) can be expressed entirely in terms of the Hessians (106) in the form

$$K = -\frac{1}{2\pi c}\sqrt{|\det(\mathbf{M}'+\mathbf{M}'')|}\;\frac{\displaystyle\int_0^\infty \omega^3|\dot m(\omega)|^2\sin\Phi\,d\omega}{\displaystyle\int_0^\infty \omega^2|\dot m(\omega)|^2\,d\omega}\,, \tag{108}$$

where

$$\Phi = \frac{1}{2}\,\omega \mathbf{q}^{\mathrm{T}} \cdot (\mathbf{M}' + \mathbf{M}'') \cdot \mathbf{q} - [\mathrm{sig}\,(\mathbf{M}' + \mathbf{M}'') - 2]\pi/4\,. \tag{109}$$

The paraxial kernel of a differential traveltime measurement $\delta(\Delta T) = \delta(T_{\mathrm{B}} - T_{\mathrm{A}})$ is obviously the difference of the individual paraxial kernels:

$$K^{\mathrm{B-A}} = K^{\mathrm{B}} - K^{\mathrm{A}} \quad \text{if} \quad M_{\mathrm{A}} = M_{\mathrm{B}}\,. \tag{110}$$

For any compound ray such as *PP*, *SS*, *PcP* or *ScS*, there may be more than perpendicular projection point $\boldsymbol{\xi}$ for scatterers $\mathbf{x}$ situated near the reflecting boundary; in that case, the result (108) must be replaced by a *sum* over all such points $\boldsymbol{\xi} = (0, 0, l)$. It is immaterial in the context of the present approximation whether the leading factor $c = \sqrt{c'c''}$ in (108) is evaluated at the scatterer $\mathbf{x}$ or at $\boldsymbol{\xi}$; we adopt the former alternative, setting $c = c(q_1, q_2, l)$, since our numerical comparisons in Banana–Doughnut II show that this choice leads to a slight improvement in the agreement with the 'exact' ray-theoretical kernel (78).

6.6 Summary of the computational procedure

To conclude this section, we outline the steps needed to compute a paraxial kernel K, for comparison with the 'exact' ray-theoretical algorithm outlined in Section 5.3.

(1) Trace the geometrical ray corresponding to the phase of interest from the source $\mathbf{s}$ to the receiver $\mathbf{r}$.

(2) Specify the position of every potential scattering point in ray-centred coordinates, $\mathbf{x} = (q_1, q_2, l)$.

(3) Compute the forward and backward traveltime Hessians $\mathbf{M}'$ and $\mathbf{M}''$ at every point $\boldsymbol{\xi} = (0, 0, l)$ along the central ray.

(4) Evaluate the kernel (108)–(109), allowing for multiple projections of $\mathbf{x} = (q_1, q_2, l)$ onto $\boldsymbol{\xi} = (0, 0, l)$ if necessary.

Only a single numerically intensive two-point ray trace is required—from the source $\mathbf{s}$ to the receiver $\mathbf{r}$. Once this central ray has been determined, the Hessians $\mathbf{M}'$ and $\mathbf{M}''$ can be found with a few additional one-time integrations. We give a detailed algorithm for computing $\mathbf{M}'$ and $\mathbf{M}''$ in a spherically symmetric earth in Appendix A. Among other things, we show there how to account for the jumps in these quantities at the boundaries Σ.

7 REDUCTION TO RAY THEORY

The Jacobian of the transformation from (x_1, x_2, x_3) to ray-centred coordinates (q_1, q_2, l) is $1 + q_i\partial_i c$ (Červený & Hron 1980; Červený 1985). Written out explicitly, the 3-D integral in eq. (107) is therefore

$$\delta T = -\frac{1}{2\pi}\int_0^L dl \iint_{-\infty}^{\infty} dq_1\,dq_2\,(1 + q_i\partial_i c)\,c^{-2}\delta c \times \sqrt{|\det(\mathbf{M}' + \mathbf{M}'')|}\left[\frac{\int_0^\infty \omega^3 |\dot m(\omega)|^2 \sin\Phi\,d\omega}{\int_0^\infty \omega^2 |\dot m(\omega)|^2\,d\omega}\right]. \tag{111}$$

The limits $\pm\infty$ on the transverse integrals over q_1, q_2 are purely formal; in practice, the kernel K is negligible except within the first few Fresnel zones about the central ray. If the dominant frequency $\bar\omega$ in the source-time power spectrum $|\dot m(\omega)|^2$ is sufficiently high, or, equivalently, the lateral scale length of the wave-speed heterogeneity is sufficiently great, we can replace the quantity $(1 + q_i\partial_i c)\,c^{-2}\delta c$ on the top line of (111) by its value $c(0, 0, l)^{-2}\delta c(0, 0, l)$ on the central ray. The order of q_1, q_2 and ω integration may then be interchanged, with the result

$$\delta T = -\int_0^L dl\, c(0, 0, l)^{-2}\delta c(0, 0, l) \times \left[\frac{\int_0^\infty \omega^3 |\dot m(\omega)|^2 \sqrt{|\det(\mathbf{M}' + \mathbf{M}'')|}\iint_{-\infty}^{\infty} \sin\Phi\,dq_1\,dq_2\,d\omega}{2\pi\int_0^\infty \omega^2 |\dot m(\omega)|^2\,d\omega}\right]. \tag{112}$$

The quantity in brackets is unity, by virtue of the Gaussian integral identity

$$\iint_{-\infty}^{\infty} \sin\Phi\,dq_1\,dq_2 = \frac{2\pi}{\omega\sqrt{|\det(\mathbf{M}' + \mathbf{M}'')|}}\,. \tag{113}$$

The traveltime perturbation (111) therefore reduces in this *stationary-phase approximation* to

$$\delta T = -\int_0^L c(0, 0, l)^{-2}\delta c(0, 0, l)\,dl\,. \tag{114}$$

This is, of course, precisely the first-order traveltime shift predicted by geometrical ray theory:

$$\delta T_{\mathrm{ray}} = -\int_{\mathbf{s}}^{\mathbf{r}} c^{-2}\delta c\,dl\,. \tag{115}$$

Fermat's principle guarantees that the change in the traveltime due to the change in the ray path between a fixed source $\mathbf{s}$ and receiver $\mathbf{r}$ is of second order in δc; this allows the first-order perturbation of (9) to be calculated by integrating along the unperturbed ray. The reduction of eqs (77)–(78) and (107)–(109) to linearized ray theory (115) in the limit $\bar\omega \to \infty$ is no surprise, inasmuch as Coates & Chapman (1990) have previously used (113) to show that the Born moment tensor response (45)–(46) is consistent with ray theory in the same approximation.

8 OVERLAPPING PHASES

There are numerous instances in which there may be more than one geometrical phase arriving within the cross-correlation time window $t_1 \le t \le t_2$. In the case of a shallow-focus source, for example, the waveforms of the 'direct' *P* and *S* arrivals may be contaminated by a superposition of later-arriving phases such as *pP*, *sP* and *sS*, *pS*. The pulse shapes of *PP* and *SS* may likewise be influenced by interference from precursory phases such as the sub-Mohorovičić reflections *PmP* and *SmS*. We extend our analysis to find 3-D Fréchet kernels for such interfering or overlapping phases in this section.

8.1 Two-phase interference

Suppose first that the unperturbed frequency-domain response during the time interval of interest $t_1 \le t \le t_2$ is a superposition of two interfering phases:

$$s(\omega) = s_1(\omega) + s_2(\omega)\,. \tag{116}$$

Each of the two signals $s_j(\omega)$, $j=1, 2$ in (116) has a JWKB representation of the form

$$s_j(\omega)=\frac{1}{4\pi}\,[A_j\mathscr{R}_j^{-1}\dot{m}(\omega)\exp i(-\omega T_j+M_j\pi/2)]\,, \tag{117}$$

where we have abbreviated

$$A_j=\Lambda_j\Upsilon_j\Pi_j \tag{118}$$

for simplicity in what follows. The perturbed response $\delta s(\omega)$ is regarded as a double sum (55) over *all possible* rays′ and rays″, including concatenations of the same 'type' as the two unscattered source-to-receiver paths, ray_1 and ray_2. To find the Fréchet kernel governing such a pair of overlapping phases, we insert (116)–(117) and (55) into eq. (66), and systematically make use of the full panoply of forward-scattering and paraxial approximations, as before. We spare the reader the details of this calculation, and simply give the final result, which may be most conveniently expressed using the condensed notation

$$\Delta T_j=\frac{1}{2}\,\mathbf{q}^{\mathrm{T}}\cdot(\mathbf{M}_j'+\mathbf{M}_j'')\cdot\mathbf{q}\,, \tag{119}$$

$$\Delta M_j=\frac{1}{2}\,[\mathrm{sig}\,(\mathbf{M}_j'+\mathbf{M}_j'')-2]\,, \tag{120}$$

where $\mathbf{M}_1'$, $\mathbf{M}_1''$ and $\mathbf{M}_2'$, $\mathbf{M}_2''$ are the forward and backward Hessians along ray_1 and ray_2, respectively. The kernel K in the representation (107) of δT is replaced by

$$\begin{aligned}K_{1+2}=-\frac{1}{2\pi cD}\int_0^\infty \omega^3|\dot{m}(\omega)|^2\\ \times[A_1^2\mathscr{R}_1^{-2}\sqrt{|\det(\mathbf{M}_1'+\mathbf{M}_1'')|}\,\sin\Phi_{11}\\ +A_1A_2\mathscr{R}_1^{-1}\mathscr{R}_2^{-1}\sqrt{|\det(\mathbf{M}_1'+\mathbf{M}_1'')|}\,\sin\Phi_{12}\\ +A_2A_1\mathscr{R}_2^{-1}\mathscr{R}_1^{-1}\sqrt{|\det(\mathbf{M}_2'+\mathbf{M}_2'')|}\,\sin\Phi_{21}\\ +A_2^2\mathscr{R}_2^{-2}\sqrt{|\det(\mathbf{M}_2'+\mathbf{M}_2'')|}\,\sin\Phi_{22}]\,d\omega\,,\end{aligned} \tag{121}$$

where

$$\Phi_{11}=\omega\,\Delta T_1-(\Delta M_1)\pi/2\,, \tag{122}$$

$$\Phi_{12}=\omega(\Delta T_1+T_1-T_2)-(\Delta M_1+M_1-M_2)\pi/2\,, \tag{123}$$

$$\Phi_{21}=\omega(\Delta T_2+T_2-T_1)-(\Delta M_2+M_2-M_1)\pi/2\,, \tag{124}$$

$$\Phi_{22}=\omega\,\Delta T_2-(\Delta M_2)\pi/2 \tag{125}$$

and

$$\begin{aligned}D=\int_0^\infty \omega^2|\dot{m}(\omega)|^2\{A_1^2\mathscr{R}_1^{-2}+A_2^2\mathscr{R}_2^{-2}+2A_1A_2\\ \times\mathscr{R}_1^{-1}\mathscr{R}_2^{-1}\cos[\omega(T_1-T_2)-(M_1-M_2)\pi/2]\}\,d\omega\,.\end{aligned} \tag{126}$$

The four terms in (121) and (122)–(125) account for the effects of type-1 and type-2 scattered waves upon the unperturbed pulses $s_1(t)$ and $s_2(t)$, respectively.

8.2 Multiple-phase interference

It is a straightforward matter to generalize the above result to a signal consisting of more than two overlapping phases,

$$s(\omega)=s_1(\omega)+s_2(\omega)+\,\cdots\,, \tag{127}$$

each of the form (117). The Fréchet kernel relating the cross-correlation traveltime shift δT to the fractional wave-speed perturbation $\delta c/c$ in that case is

$$\begin{aligned}K_\Sigma=-\frac{1}{2\pi cD}\int_0^\infty \omega^3|\dot{m}(\omega)|^2\\ \times\sum_j\sum_k A_jA_k\mathscr{R}_j^{-1}\mathscr{R}_k^{-1}\sqrt{|\det(\mathbf{M}_j'+\mathbf{M}_j'')|}\\ \times\sin[\omega(\Delta T_j+T_j-T_k)-(\Delta M_j+M_j-M_k)\pi/2]\,d\omega\,,\end{aligned} \tag{128}$$

where

$$\begin{aligned}D=\int_0^\infty \omega^2|\dot{m}(\omega)|^2\sum_j\sum_k A_jA_k\mathscr{R}_j^{-1}\mathscr{R}_k^{-1}\\ \times\cos[\omega(T_j-T_k)-(M_j-M_k)\pi/2]\,d\omega\,.\end{aligned} \tag{129}$$

The subscript Σ in (128) serves as a reminder that this is the kernel for a superposition of interfering phases $j=1, 2, \ldots$. The ray paths followed by the phases in both (121)–(126) and (128)–(129) are presumed to be adjacent, so that slight differences in the attenuation times T_1^*, T_2^*, ... can be ignored.

8.3 Limiting cases

Suppose that all of the phases in (127) have the same pulse shape, $M_j=M_k$, and are well separated in the time domain, i.e.

$$\bar{\omega}|T_j-T_k|\gg 1\quad\text{for}\quad j\neq k\,. \tag{130}$$

The oscillatory cross-terms are then negligible as a result of destructive interference between adjacent frequencies ω and $\omega+d\omega$, so that (128)–(129) reduces to

$$K_\Sigma=\sum_j\left(\frac{A_j^2\mathscr{R}_j^{-2}}{\sum_k A_k^2\mathscr{R}_k^{-2}}\right)K_j\,. \tag{131}$$

The multiphase kernel K_Σ in this approximation is a sum of individual kernels K_j, each weighted by the relative (amplitude)^2 of the associated far-field pulse. This makes intuitive sense, since what one is then measuring is an average traveltime shift δT of a number of distinct arrivals in a (presumably long) time interval $t_1\le t\le t_2$. Strong pulses will obviously have a greater influence upon this average traveltime than weak ones. The condition (130) prevails, for example, for the direct and depth phases S and sS, whenever the source is deep enough for these two arrivals to be isolated in the seismogram. The kernel (131) for such a deep-source traveltime shift δT_{S+sS} is

$$\begin{aligned}K_{S+sS}=\left(\frac{A_S^2\mathscr{R}_S^{-2}}{A_S^2\mathscr{R}_S^{-2}+A_{sS}^2\mathscr{R}_{sS}^{-2}}\right)K_S\\ +\left(\frac{A_{sS}^2\mathscr{R}_{sS}^{-2}}{A_S^2\mathscr{R}_S^{-2}+A_{sS}^2\mathscr{R}_{sS}^{-2}}\right)K_{sS}\,.\end{aligned} \tag{132}$$

In practice, of course, one would never measure a single average traveltime for two such well-separated phases; instead, one would window the two phases separately, and measure the individual time shifts δT_S and δT_{sS}.

In the opposite limit of a surface focus source, the phases S and sS arrive simultaneously: $T_S=T_{sS}$. A common factor

of $A_S^2\mathscr{R}_S^{-2}+A_{sS}^2\mathscr{R}_{sS}^{-2}+2A_SA_{sS}\mathscr{R}_S^{-1}\mathscr{R}_{sS}^{-1}$ in the numerator and denominator of (121) then cancels, so that the kernel for δT_{S+sS} reduces to

$$K_{S+sS}=K_S=K_{sS}\,. \tag{133}$$

In other words, the kernel for the simultaneously arriving S and sS phases is identical to that for either of the two phases considered individually. This too is in accord with elementary physical intuition.

9 CONCLUSIONS

The most important results in this paper are eqs (108) and (110), giving the paraxial Fréchet kernels K for an absolute traveltime measurement δT and a differential traveltime measurement $\delta(\Delta T)$, respectively. The kernel (108) for a single, well-isolated seismic phase depends only upon the sum $\mathbf{M}'+\mathbf{M}''$ of forward and backward traveltime Hessians along the central geometrical ray. Forward Rayleigh scattering, wave-front healing and other diffraction effects give rise to a frequency-dependent off-path dependence proportional to the quantity $\sin\{\frac{1}{2}\omega\mathbf{q}^{\mathrm{T}}\cdot(\mathbf{M}'+\mathbf{M}'')\cdot\mathbf{q}-[\mathrm{sig}\,(\mathbf{M}'+\mathbf{M}'')-2]\pi/4\}$, where $\mathbf{q}$ is the perpendicular distance of a scatterer $\mathbf{x}$ from the ray. The Fréchet kernel for a differential traveltime measurement $\delta(\Delta T)=\delta(T_{\mathrm{B}}-T_{\mathrm{A}})$ of two 'identical-pulse-shape' phases is simply the difference of the single-phase kernels: $K^{\mathrm{B}-\mathrm{A}}=K^{\mathrm{B}}-K^{\mathrm{A}}$. These results provide a natural extension of linearized geometrical ray theory to finite-frequency waves. The frequency content of the cross-correlated pulse is explicitly accounted for by the presence of the source time power spectrum $|\dot{m}(\omega)|^2$ in the representation (108) of a single-phase kernel. Destructive interference among adjacent frequencies ω and $\omega+d\omega$ confines the strong sensitivity to the vicinity of the first Fresnel zone surrounding the central ray. The Fréchet kernel of very high-frequency waves is a very slender hollow banana; lower-frequency waves are, on the other hand, sensitive to wave-speed heterogeneity $\delta c/c$ farther off the ray. To quantify these remarks, we present a number of illustrative examples of both absolute and differential traveltime Fréchet kernels in the paper that follows, Banana–Doughnut II.

ACKNOWLEDGMENTS

The possibility that adjacent-path interfering phases might affect the cross-correlation traveltimes of *P*, *S* and *PP*, *SS* waves was pointed out to us by Li Zhao. Financial support for this work has been provided by the US National Science Foundation under Grants EAR-9505677 and EAR-9725496.

REFERENCES

Brune, J.N., Nafe, J.E. & Alsop, L.E., 1961. The polar phase shift of surface waves on a sphere, *Bull. seism. Soc. Am.,* **51,** 247–257.

Červený, V., 1985. The application of ray tracing to the numerical modeling of seismic wavefields in complex structures, in *Seismic Shear Waves, Part A: Theory, Handbook of Geophysical Exploration,* Vol. 15A, pp. 1–124, ed. Dohr, G.P., Geophysical Press, London.

Červený, V. & Hron, F., 1980. The ray series method and dynamic ray tracing systems for 3-D inhomogeneous media, *Bull. seism. Soc. Am.,* **70,** 47–77.

Červený, V., Molotkov, I.A. & Pšenčík, 1977. *Ray Method in Seismology,* Univerzita Karlova, Praha.

Coates, R.T. & Chapman, C.H., 1990. Ray perturbation theory and the Born approximation, *Geophys. J. Int.,* **100,** 379–392.

Dahlen, F.A. & Tromp, J., 1998. *Theoretical Global Seismology,* Princeton University Press, Princeton.

Dziewonski, A.M., 1984. Mapping the lower mantle: determination of lateral heterogeneity in P velocity up to degree and order 6, *J. geophys. Res.,* **89,** 5929–5952.

Grand, S.P., 1994. Mantle shear structure beneath the Americas and surrounding oceans, *J. geophys. Res.,* **99,** 11 591–11 621.

Hudson, J.A., 1977. Scattered waves in the coda of P, *J. Geophys.,* **43,** 359–374.

Hung, S.-H., Dahlen, F.A. & Nolet, G., 2000. Fréchet kernels for finite-frequency traveltimes—II. Examples, *Geophys. J. Int.,* **141,** 175–203 (this issue).

Inoue, H., Fukao, Y., Tanabe, K. & Ogata, Y, 1990. Whole mantle P-wave travel time tomography, *Phys. Earth planet. Inter.,* **59,** 294–328.

Kravstov, Yu.A. & Orlov, Yu.I., 1990. *Geometrical Optics of Inhomogeneous Media,* Springer-Verlag, New York.

Kuo, B.-Y., Forsyth, D.W. & Wysession, M., 1987. Lateral heterogeneity and azimuthal anisotropy in the North Atlantic determined from SS-S differential traveltimes, *J. geophys. Res.,* **92,** 6421–6436.

Luo, Y. & Schuster, G.T., 1991. Wave-equation traveltime tomography, *Geophysics,* **56,** 645–653.

Marquering, H., Dahlen, F.A. & Nolet, G., 1999. Three-dimensional sensitivity kernels for finite-frequency traveltimes: the banana-doughnut paradox, *Geophys. J. Int.,* **137,** 805–815.

Masters, G., Johnson, S., Laske, G. & Bolton, H., 1996. A shear-velocity model of the mantle, *Phil. Trans. R. Soc. Lond.,* A**354,** 1385–1411.

Pulliam, R.J., Vasco, D.W. & Johnson, L.R., 1993. Tomographic inversions for mantle P wave velocity structure based on the minimization of l2 and l1 norms of International Seismological Centre travel time residuals, *J. geophys. Res.,* **98,** 699–734.

Sheehan, A. & Solomon, S., 1991. Joint inversion of shear wave travel-time residuals and geoid and depth anomalies for long-wavelength variations in upper mantle temperature and composition along the Mid-Atlantic Ridge, *J. geophys. Res.,* **96,** 19 981–20 009.

Snieder, R. & Chapman, C.H., 1998. The reciprocity properties of geometrical spreading, *Geophys. J. Int.,* **132,** 89–95.

Su, W.-J. & Dziewonski, A.M., 1992. On the scale of mantle heterogeneity, *Phys. Earth planet. Inter.,* **74,** 29–54.

VanDecar, J. & Crosson, R., 1990. Determination of teleseismic relative phase arrival times using multi-channel cross-correlation and least squares, *Bull. seism. Soc. Am.,* **80,** 150–159.

Van der Hilst, R.D., Widiyantoro, S. & Engdahl, E.R., 1997. Evidence for deep mantle circulation from global tomography, *Nature,* **386,** 578–584.

Woodward, R.L. & Masters, G., 1991. Global upper mantle structure from long-period differential traveltimes, *J. geophys. Res.,* **96,** 6351–6377.

Wu, R.S. & Aki, K., 1985. Elastic wave scattering by a random medium and the small-scale inhomogeneities in the lithosphere, *J. geophys. Res.,* **90,** 10 261–10 273.

Zhao, L. & Dahlen, F.A., 1996. Mode-sum to ray-sum transformation in a spherical and aspherical Earth, *Geophys. J. Int.,* **126,** 389–412.

APPENDIX A: SPHERICAL EARTH KERNELS

Consider a spherically symmetric earth model of radius a, with a prescribed radial variation in wave speed $c(r)$. We assume that $c(r)$ is smooth everywhere within $0\le r\le a$, except for jump discontinuities at a number of internal solid–solid interfaces $r=d_{\mathrm{SS}}$ and fluid–solid interfaces $r=d_{\mathrm{FS}}$. We denote the union of all discontinuities, including the outer free surface $r=a$, by $d=a\cup d_{\mathrm{SS}}\cup d_{\mathrm{FS}}$. The spherical polar coordinates of an

arbitrary point within the Earth will be denoted by $\mathbf{x}=(r, \theta, \phi)$, where θ is the colatitude and ϕ is the longitude, as usual. We describe a practical and economical algorithm for computing the paraxial Fréchet kernel K of an arbitrary phase within such a piecewise smooth, spherical earth model in this Appendix.

A1 Kinematic ray tracing

Seismic rays within a spherical earth model are confined to the source–receiver great-circle plane. Kinematic ray tracing is most readily performed using a rotated coordinate system, in which the source and receiver are situated upon the equator, at points

$$\mathbf{s}=(r_s, \pi/2, 0), \qquad \mathbf{r}=(a, \pi/2, \Delta). \tag{A1}$$

The quantity $h=a-r_s$ is the source depth, and Δ is the angular epicentral distance, as illustrated in Fig. A1. The receiver is assumed to be situated on the earth's surface, $r_r=a$, since that is the only case of practical interest in global seismology. The incidence angle $0\le i\le\pi$ is measured downwards from the local vertical $\hat{\mathbf{r}}$, so that the unit wave vector along either a downgoing or upgoing leg of a ray is given by

$$\hat{\mathbf{k}}=\hat{\mathbf{r}}\cos i+\hat{\boldsymbol{\phi}}\sin i. \tag{A2}$$

The *SV* and *SH* polarization vectors are chosen to point upwards and to the right of an eastward-propagating wave:

$$\hat{\mathbf{q}}_1=\hat{\mathbf{q}}_{SV}=\hat{\mathbf{r}}\sin i-\hat{\boldsymbol{\phi}}\cos i, \qquad \hat{\mathbf{q}}_2=\hat{\mathbf{q}}_{SH}=\hat{\boldsymbol{\theta}}. \tag{A3}$$

With this choice, the *SV*, *SH*, *P* polarization triad is right-handed, $(\hat{\mathbf{q}}_1\times\hat{\mathbf{q}}_2)\cdot\hat{\mathbf{k}}=(\hat{\mathbf{q}}_{SV}\times\hat{\mathbf{q}}_{SH})\cdot\hat{\mathbf{k}}=1$, as shown.

The three quantities r, i and c all vary as we move from one point to another; however, as is well known, the ray parameter

$$p=\frac{r\sin i}{c} \tag{A4}$$

has the same value everywhere along a geometrical ray. The path r, ϕ of a ray in the equatorial plane $\theta=\pi/2$ may be determined by integrating the three first-order differential equations (Dahlen & Tromp 1998, Section 15.1.2)

$$\frac{dr}{dl}=\cos i, \qquad \frac{d\phi}{dl}=r^{-1}\sin i, \qquad \frac{di}{dl}=pr^{-1}(\dot{c}-c/r), \tag{A5}$$

where the dot denotes the radial derivative, $\dot{c}=dc/dr$. The independent variable, which is the arclength l along the ray, may be eliminated from (A5), leading to a pair of coupled equations,

$$\frac{dr}{d\phi}=r\cot i, \qquad \frac{di}{d\phi}=r\dot{c}/c-1. \tag{A6}$$

Wherever a ray intersects an interface $r=d$, the differential equations (A6) must be supplemented by the continuity conditions

$$[r]^+_-=0, \qquad [c^{-1}\sin i]^+_-=0. \tag{A7}$$

The jump notation $[\cdot]^+_-$ throughout this Appendix has a slightly different meaning than elsewhere in the paper: the signs + and − refer to the outgoing and incoming ray paths, respectively. In the case of a transmitted wave such as *PKP* or *SKS*, the outgoing and incoming rays are on opposite sides of the boundary, whereas in the case of a reflection such as *PP*, *SS*, *PcP* or *ScS*, they are on the same side. Even in the latter case, the wave speeds $c_\pm$ need not be the same on the two legs of a converted phase such as *PS*, *SP*, *PcS* or *ScP*. The first of the two continuity conditions (A7) simply states that the boundary is immobile, whereas the second is Snell's law.

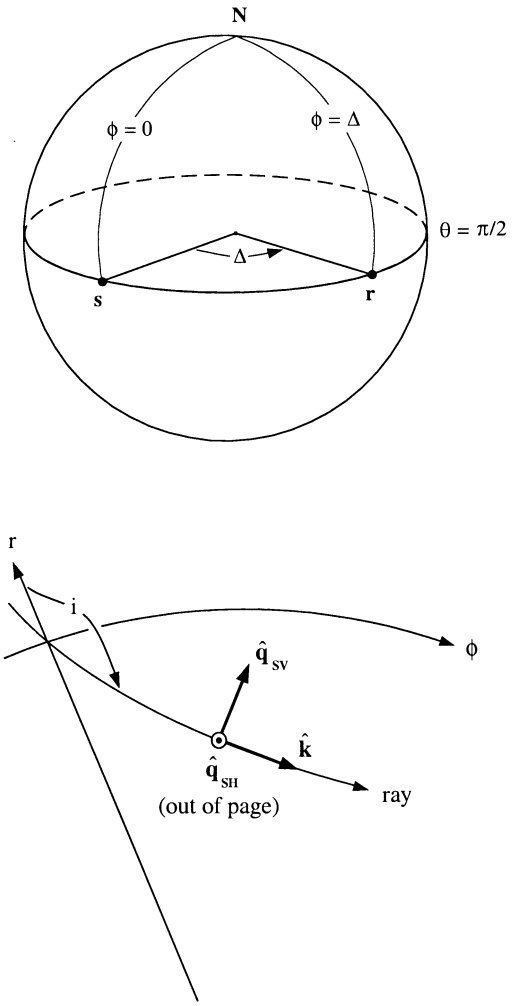

Figure A1. (Top) Kinematic and dynamic ray tracing in a spherically symmetric earth is conducted using a rotated coordinate system, with the source **s** and receiver **r** situated upon the equator, at longitudes $\phi=0$ and $\phi=\Delta$, respectively. Rays are confined to the equatorial plane, $\theta=\pi/2$. (Bottom) Cross-section of the ray plane, showing the *P*-wave polarization, or unit wave vector, $\hat{\mathbf{k}}$, and the vertical and horizontal *S*-wave polarizations $\hat{\mathbf{q}}_{SV}$ and $\hat{\mathbf{q}}_{SH}$. The position of an arbitrary point along the ray is completely specified in terms of the local radius r and longitude $0\le\phi\le\Delta$. The angle of incidence i is in the range $\pi\ge i\ge\pi/2$ on every downgoing leg and $\pi/2\ge i\ge 0$ on every upgoing leg of a simple or compound ray.

To trace or 'shoot' a ray from the source **s**, we integrate (A6) subject to the boundary conditions (A7) on $r=d$ and the initial conditions

$$r(0)=r_s, \qquad i(0)=i_s. \tag{A8}$$

Iteration is required to find the initial take-off angle i_s at the source that enables the ray to 'hit' the receiver **r**; the final condition is that the ray must arrive at the surface of the earth after having travelled exactly the specified epicentral distance, i.e.

$$r(\Delta)=a. \tag{A9}$$

Any standard root-finding procedure can be used to solve this two-point ray-tracing problem. By using ϕ rather than l as the independent variable, we restrict the search to one rather than two dimensions.

A2 Dynamic ray tracing

The only remaining ingredients needed to compute the paraxial Fréchet kernel (107)–(108) are the forward and backward Hessian matrices $\mathbf{M}'$ and $\mathbf{M}''$. In a spherically symmetric earth model, these matrices are diagonal:

$$\mathbf{M}' = \begin{pmatrix} M_1' & 0 \\ 0 & M_2' \end{pmatrix}, \qquad \mathbf{M}'' = \begin{pmatrix} M_1'' & 0 \\ 0 & M_2'' \end{pmatrix}. \tag{A10}$$

Here, as elsewhere in this paper, $\mathbf{M}'$ and $\mathbf{M}''$ are expressed in ray-centred coordinates; the difference (91) in traveltime from the source $\mathbf{s}=(0, 0, 0)$ to the receiver $\mathbf{r}=(0, 0, L)$, along a path passing through a scatterer $\mathbf{x}=(q_1, q_2, l)$ or through the nearest point on the central ray $\boldsymbol{\xi}=(0, 0, l)$, is given by

$$T'+T''-T=\frac{1}{2}(M_1'+M_1'')q_1^2+\frac{1}{2}(M_2'+M_2'')q_2^2. \tag{A11}$$

Once the central kinematic ray has been determined, the four quantities M_1', M_2' and M_1'', M_2'' can be computed with a few additional initial-value integrations. We focus first upon the Hessian $\mathbf{M}'$ measured from the source $\mathbf{s}$, rewriting it as

$$\mathbf{M} = \begin{pmatrix} M_1 & 0 \\ 0 & M_2 \end{pmatrix}, \tag{A12}$$

where the primes have been dropped for simplicity.

As discussed in the body of the paper, $\mathbf{M}$ satisfies the forward Ricatti equation,

$$\frac{d\mathbf{M}}{dl}+c\mathbf{M}^2+c^{-2}\mathbf{V}=\mathbf{0}. \tag{A13}$$

The wave-speed second-derivative matrix $\mathbf{V}$ in spherical polar coordinates is $\mathbf{V}=\ddot{c}\hat{\mathbf{r}}\hat{\mathbf{r}}+r^{-1}\dot{c}(\hat{\boldsymbol{\theta}}\hat{\boldsymbol{\theta}}+\hat{\boldsymbol{\phi}}\hat{\boldsymbol{\phi}})$, so that in ray-centred coordinates it is

$$\mathbf{V} = \begin{pmatrix} \ddot{c}\sin^2 i+r^{-1}\dot{c}\cos^2 i & 0 \\ 0 & r^{-1}\dot{c} \end{pmatrix}. \tag{A14}$$

Eq. (A13) must be solved subject to the point-source initial condition at $\boldsymbol{\xi}\to\mathbf{s}$:

$$\mathbf{M}\to c_s l^{-1}\mathbf{I} \text{ as } l\to 0, \tag{A15}$$

where $\mathbf{I}$ is the 2×2 identity.

In addition, $\mathbf{M}$ must satisfy a condition guaranteeing that wave fronts in the vicinity of the central ray are continuous across boundaries. Upon specializing the analysis of Červený & Hron (1980) and Červený (1985) to the case of a spherically symmetric earth, we obtain the requisite boundary condition, analogous to (A7),

$$[\mathbf{R}^{\mathrm{T}}\cdot\mathbf{M}\cdot\mathbf{R}-c^{-1}\cos i\,\mathbf{D}+\mathbf{E}]_-^+=\mathbf{0}. \tag{A16}$$

All three matrices $\mathbf{R}^{\mathrm{T}}\cdot\mathbf{M}\cdot\mathbf{R}$, $\mathbf{D}$ and $\mathbf{E}$ in eq. (A16) are expressed in θ, ϕ coordinates, that is, on the boundary $r=d$. The orthogonal matrix

$$\mathbf{R} = \begin{pmatrix} -\cos i & 0 \\ 0 & 1 \end{pmatrix} = \mathbf{R}^{\mathrm{T}} \tag{A17}$$

transforms the ray-centred Hessian $\mathbf{M}$ to these boundary coordinates:

$$\mathbf{R}^{\mathrm{T}}\cdot\mathbf{M}\cdot\mathbf{R} = \begin{pmatrix} M_1\cos^2 i & 0 \\ 0 & M_2 \end{pmatrix}. \tag{A18}$$

The matrices $\mathbf{D}$ and $\mathbf{E}$ account for the curvature and the gradient in wave speed $\dot{c}_\pm$ on the outgoing and incoming sides of the boundary, respectively. The first is simply the boundary curvature matrix $\mathbf{D}=r^{-1}(\hat{\boldsymbol{\theta}}\hat{\boldsymbol{\theta}}+\hat{\boldsymbol{\phi}}\hat{\boldsymbol{\phi}})$, or, equivalently,

$$\mathbf{D} = r^{-1}\begin{pmatrix} 1 & 0 \\ 0 & 1 \end{pmatrix}, \tag{A19}$$

whereas the second is given by

$$\mathbf{E} = c^{-2}\dot{c}\cos i\,\sin^2 i\begin{pmatrix} 1 & 0 \\ 0 & 0 \end{pmatrix}. \tag{A20}$$

Upon substituting (A12) and (A14) we can write (A13) as a pair of uncoupled scalar equations:

$$\frac{dM_1}{d\phi}+p^{-1}r^2M_1^2+pc^{-1}(\ddot{c}+r^{-1}\dot{c}\cot^2 i)=0, \tag{A21}$$

$$\frac{dM_2}{d\phi}+p^{-1}r^2M_2^2+p^{-1}rc^{-3}\dot{c}=0, \tag{A22}$$

where we have used (A4) and the second of eqs (A5) to transform the independent variable from the arclength l to the longitude ϕ, for consistency with (A6). We must solve (A21)–(22), together with the jump conditions

$$[M_1\cos^2 i-r^{-1}c^{-1}\cos i+c^{-2}\dot{c}\cos i, \sin^2 i]_-^+=0, \tag{A23}$$

$$[M_2-r^{-1}c^{-1}\cos i]_-^+=0 \tag{A24}$$

on the boundaries $r=d$, subject to the initial conditions

$$M_1,\, M_2\to c_s l^{-1} \text{ as } l\to 0 \tag{A25}$$

at the source $\boldsymbol{\xi}\to\mathbf{s}$. The two components M_1, M_2 govern the geometrical spreading within the equatorial ray plane and perpendicular to the ray plane, respectively. The diagonal character of the various matrices $\mathbf{M}$, $\mathbf{V}$, $\mathbf{R}$, $\mathbf{D}$ and $\mathbf{E}$ renders these two spreading directions independent in a spherically symmetric earth.

A3 Numerical integration

Direct numerical integration of eqs (A21)–(A24) is impractical because of the divergent character of the initial conditions (A25). A convenient computational scheme can be based upon the decomposition (Červený 1985)

$$\mathbf{M}=\mathbf{P}\cdot\mathbf{Q}^{-1}. \tag{A26}$$

This reduces the Ricatti equation (A13) to a pair of coupled first-order linear equations:

$$\frac{d\mathbf{P}}{dl}=-c^{-2}\mathbf{V}\cdot\mathbf{Q}, \qquad \frac{d\mathbf{Q}}{dl}=c\mathbf{P}. \tag{A27}$$

In a spherically symmetric earth, both matrices in (A26) are diagonal:

$$\mathbf{P}=\begin{pmatrix} P_1 & 0 \\ 0 & P_2 \end{pmatrix}, \qquad \mathbf{Q}=\begin{pmatrix} Q_1 & 0 \\ 0 & Q_2 \end{pmatrix}. \tag{A28}$$

The elements of **M**, **P** and **Q** are simply related by

$$M_1=P_1/Q_1\,, \qquad M_2=P_2/Q_2\,. \tag{A29}$$

The governing equations (A27) are likewise equivalent to the quartet of scalar relations

$$\frac{dP_1}{d\phi}=-pc^{-1}(\ddot{c}+r^{-1}\dot{c}\cot^2 i)Q_1\,, \qquad \frac{dQ_1}{d\phi}=p^{-1}r^2P_1\,, \tag{A30}$$

$$\frac{dP_2}{d\phi}=-p^{-1}rc^{-3}\dot{c}Q_2\,, \qquad \frac{dQ_2}{d\phi}=p^{-1}r^2P_2\,, \tag{A31}$$

where we have again used (A4) and the second of eqs (A5) to change the independent variable from l to ϕ, as in (A21)–(A22). The jump conditions on P_1, P_2, Q_1, Q_2 equivalent to (23)–(A24) are

$$[\cos i\,P_1+(p^2r^{-2}\dot{c}-r^{-1}c^{-1})Q_1]^+_-=0\,, \tag{A32}$$

$$[P_2-r^{-1}c^{-1}\cos i\,Q_2]^+_-=0\,, \tag{A33}$$

$$[Q_1/\cos i]^+_-=[Q_2]^+_-=0\,. \tag{A34}$$

Eqs (A30)–(A31) and (A32)–(A34) must be solved subject to the initial conditions $\mathbf{P}(0)=\mathbf{I}$ and $\mathbf{Q}(0)=\mathbf{0}$ at the source **s**, i.e.

$$P_1(0)=P_2(0)=1\,, \qquad Q_1(0)=Q_2(0)=0\,. \tag{A35}$$

A4 Symplectic symmetry

The backward Hessian $\mathbf{M}''$ may be found by means of an analogous algorithm based upon integration of the Ricatti equation (93) from the receiver **r** to the source **s**. Alternatively, we may compute $\mathbf{M}''$ without any backward integration by exploiting the symplectic symmetry of the dynamic ray-tracing equations (Červený 1985; Dahlen & Tromp 1998, Section 15.4.10). To this end, we introduce the 4×4 propagator associated with the differential system (A27):

$$\boldsymbol{\pi}=\begin{pmatrix} \tilde{Q}_1 & 0 & Q_1 & 0 \\ 0 & \tilde{Q}_2 & 0 & Q_2 \\ \tilde{P}_1 & 0 & P_1 & 0 \\ 0 & \tilde{P}_2 & 0 & P_2 \end{pmatrix}. \tag{A36}$$

The quantities $\tilde{P}_1$, $\tilde{P}_2$ and $\tilde{Q}_1$, $\tilde{Q}_2$ satisfy the same first-order differential equations (A30)–(A31) and jump conditions (A32)–(A34) as P_1, P_2 and Q_1, Q_2; only the initial conditions (A35) are different:

$$\tilde{P}_1(0)=\tilde{P}_2(0)=0\,, \qquad \tilde{Q}_1(0)=\tilde{Q}_2(0)=1\,. \tag{A37}$$

The conditions (A37) guarantee that the matrix (A36) is a propagator, satisfying

$$\boldsymbol{\pi}(0,\,0)=\mathbf{I}\,. \tag{A38}$$

The standard concatenation and reversal properties of a propagator stipulate that

$$\boldsymbol{\pi}(\Delta,\,\phi)=\boldsymbol{\pi}(\Delta,\,0)\cdot\boldsymbol{\pi}(0,\,\phi)\,, \tag{A39}$$

$$\boldsymbol{\pi}(\phi,\,\Delta)=\boldsymbol{\pi}^{-1}(\Delta,\,\phi)\,. \tag{A40}$$

Upon combining (A39)–(A40) we obtain a representation of the sought-after propagator from the receiver in terms of the propagator from the source and its inverse:

$$\boldsymbol{\pi}(\phi,\,\Delta)=\boldsymbol{\pi}(\phi,\,0)\cdot\boldsymbol{\pi}^{-1}(\Delta,\,0)\,. \tag{A41}$$

The symplectic property of the propagator enables us to express the inverse in (A41) explicitly in the form (Červený 1985)

$$\boldsymbol{\pi}^{-1}=\begin{pmatrix} P_1 & 0 & -Q_1 & 0 \\ 0 & P_2 & 0 & -Q_2 \\ -\tilde{P}_1 & 0 & \tilde{Q}_1 & 0 \\ 0 & -\tilde{P}_2 & 0 & \tilde{Q}_2 \end{pmatrix}. \tag{A42}$$

At every point $0\le\phi\le\Delta$ between the source **s** and the receiver **r**, we define

$$P_3(\phi)=P_1(\phi)\tilde{Q}_1(\Delta)-\tilde{P}_1(\phi)Q_1(\Delta)\,, \tag{A43}$$

$$Q_3(\phi)=\tilde{Q}_1(\phi)Q_1(\Delta)-Q_1(\phi)\tilde{Q}_1(\Delta)\,, \tag{A44}$$

$$P_4(\phi)=P_2(\phi)\tilde{Q}_2(\Delta)-\tilde{P}_2(\phi)Q_2(\Delta)\,, \tag{A45}$$

$$Q_4(\phi)=\tilde{Q}_2(\phi)Q_2(\Delta)-Q_2(\phi)\tilde{Q}_2(\Delta)\,. \tag{A46}$$

A5 Forward and backward Hessians

The forward and backward Hessian matrices $\mathbf{M}'=\mathbf{M}_{\xi s}$ and $\mathbf{M}''=\mathbf{M}_{\xi r}$ are given in terms of the propagator (A36) and the four quantities (A43)–(A46) by

$$\mathbf{M}'=\begin{pmatrix} P_1/Q_1 & 0 \\ 0 & P_2/Q_2 \end{pmatrix}, \tag{A47}$$

$$\mathbf{M}''=\begin{pmatrix} P_3/Q_3 & 0 \\ 0 & P_4/Q_4 \end{pmatrix}. \tag{A48}$$

A total of four forward 2×2 integrations are needed to find $\{P_1,\,Q_1\}$, $\{P_2,\,Q_2\}$, $\{\tilde{P}_1,\,\tilde{Q}_1\}$, $\{\tilde{P}_2,\,\tilde{Q}_2\}$, and therefore the quantities $\{P_3,\,Q_3\}$, $\{P_4,\,Q_4\}$, everywhere along the central ray $\mathbf{s}\le\boldsymbol{\xi}\le\mathbf{r}$. In each of the four cases, we integrate eqs (A30)–(A31), starting with the initial conditions (A35) or (A37) at the source $\phi=0$, using a Runge–Kutta or analogous forward-stepping scheme. Upon intersecting the first boundary $r=d$, we use (A32)–(A34) to step across, continue integrating to the next boundary, and so on, until arriving at the receiver $\phi=\Delta$.

A6 Analytical results

The numerical algorithm described above suffices to determine both $\mathbf{M}'$ and $\mathbf{M}''$. However, we can go a long way towards finding these quantities entirely analytically. In particular, the factors P_2, Q_2 and M_2 governing spreading perpendicular to the ray plane are given explicitly by

$$P_2=p^{-1}c^{-1}r_s\sin(i+\phi)\,, \qquad Q_2=p^{-1}rr_s\sin\phi\,, \tag{A49}$$

$$M_2=\frac{\sin(i+\phi)}{cr\sin\phi}\,. \tag{A50}$$

It is readily verified that (A49)–(A50) satisfy all of the differential equations and jump and initial conditions (A22), (A24), (A25), (A31), (A33), (A34) and (A35). Spreading perpendicular to the ray plane is controlled primarily by the sphericity of the earth, so it is no surprise that it has such

a simple analytical description. The divergence of M_2 at $\phi=\pi, 2\pi, \ldots$ is indicative of the presence of a caustic along the straight line passing through the source **s** and its antipode. The $\pi/2$ phase shift produced by a passage through this caustic is the body wave analogue of the so-called polar phase shift of a surface wave (Brune *et al.* 1961; Dahlen & Tromp 1998, Section 11.4 and last paragraph of Section 12.5.1). The factors analogous to (A49)–(A50) along the backward ray from the receiver **r** to the source **s** are obtained by substituting $r_s \to r_r$, $\phi \to \Delta - \phi$ and $i \to \pi - i$. In particular, the forward-plus-backward sum $M_2' + M_2''$ is given by the simple expression

$$M_2' + M_2'' = \frac{p r^{-2} \sin\Delta}{\sin\phi \sin(\Delta-\phi)} \,. \tag{A51}$$

It is noteworthy that (A51) is continuous everywhere along the source–receiver ray:

$$[M_2' + M_2'']_-^+ = 0 \,. \tag{A52}$$

It is also evident that $M_2' + M_2''$ will be symmetric with respect to the source and receiver if and only if **s** and **r** are situated at the same depth, $r_s = r_r$.

The equations (A21), (A23), (A25), (A30), (A32), (A34) and (A35) governing the in-plane spreading factors P_1, Q_1 and M_1 cannot likewise be solved entirely analytically. There is, however, a conserved quantity, or readily determined integral of the in-plane motion; it is easily verified that the combination

$$r \cos i \, P_1 + (p^2 r^{-1} \dot{c} - c^{-1}) Q_1 = r_s \cos i_s \tag{A53}$$

is everywhere constant along a ray. The forward-plus-backward sum $M_1' + M_1''$ exhibits a discontinuity at every boundary intersection point $r = d$; there is, nevertheless, an analogue of the out-of-plane jump condition (A52):

$$[\cos^2 i \, (M_1' + M_1'')]_-^+ = 0 \,. \tag{A54}$$

All of the results (A49)–(A54) can be used to provide a check upon the accuracy of the numerical integration procedure.

A7 Geometrical spreading factors

The individual spreading factors $\mathscr{R} = \mathscr{R}_{rs}$, $\mathscr{R}' = \mathscr{R}_{\xi s}$ and $\mathscr{R}'' = \mathscr{R}_{\xi r}$ are not required to compute the paraxial kernel (108). However, they are a by-product of the above dynamical ray-tracing procedure; in fact (Červený 1985),

$$\mathscr{R} = c_s^{-1} \sqrt{|Q_1(\Delta) Q_2(\Delta)|} \,, \tag{A55}$$

$$\mathscr{R}' = c_s^{-1} \sqrt{|Q_1(\phi) Q_2(\phi)|} \,, \tag{A56}$$

$$\mathscr{R}'' = c_r^{-1} \sqrt{|Q_3(\phi) Q_4(\phi)|} \,. \tag{A57}$$

The results (A55)–(A57) provide an alternative means of computing the ratio (104):

$$\frac{\mathscr{R}}{c_r \mathscr{R}' \mathscr{R}''} = \sqrt{|\det(\mathbf{M}' + \mathbf{M}'')|} \,. \tag{A58}$$

Eqs (A52) and (A54) can be combined to yield the jump-condition analogue of the differential equation (94):

$$[\cos^2 i \det(\mathbf{M}' + \mathbf{M}'')]_-^+ = 0 \,. \tag{A59}$$

It is noteworthy that the dependence (A16) of the one-way jumps $[\mathbf{M}']_-^+$ and $[\mathbf{M}'']_-^+$ upon the boundary-curvature and wave-speed-gradient matrices **D** and **E** has been eliminated. The forward and backward spreading factors satisfy the continuity conditions (Dahlen & Tromp 1998, Section 12.1.7)

$$[\mathscr{R}' / \sqrt{|\cos i|}\,]_-^+ = [\mathscr{R}'' / \sqrt{|\cos i|}\,]_-^+ = 0 \,. \tag{A60}$$

The geometrical factors $1/\sqrt{|\cos i|}$ in (A60) account for the change in ray-tube area upon reflection, transmission or conversion. The left and right sides of (A58) suffer equal jumps at every boundary, inasmuch as

$$\frac{\mathscr{R}}{c_r \mathscr{R}'_+ \mathscr{R}''_+} = \frac{|\cos i_-|}{|\cos i_+|} \frac{\mathscr{R}}{c_r \mathscr{R}'_- \mathscr{R}''_-} \,, \tag{A61}$$

$$\sqrt{|\det(\mathbf{M}'_+ + \mathbf{M}''_+)|} = \frac{|\cos i_-|}{|\cos i_+|} \sqrt{|\det(\mathbf{M}'_- + \mathbf{M}''_-)|} \,. \tag{A62}$$